Condition Monitoring of Hydraulic Actuator in Wind Turbine Pitch Systems: Investigation and EKF Implementation

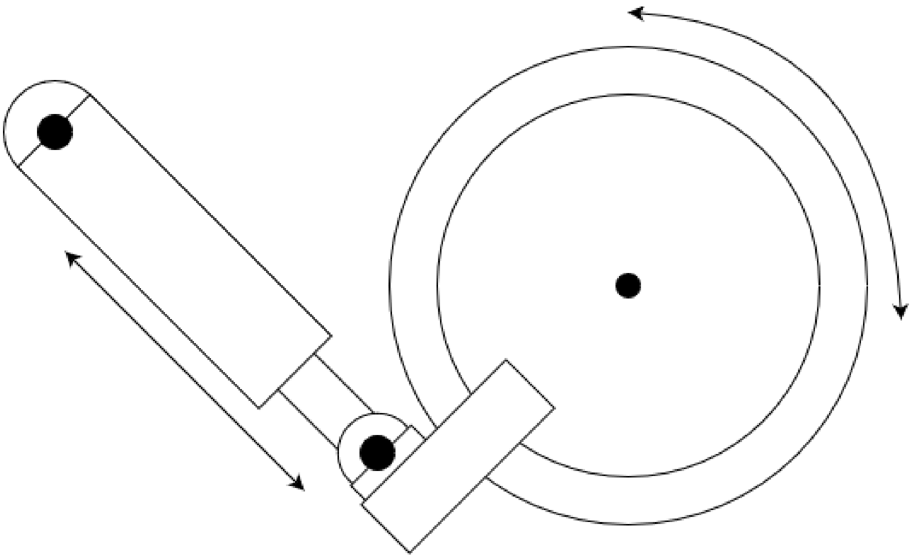

Master Thesis Project
Group MCE4-1021
Department of Energy Technology
Aalborg University
2nd June 2023

AALBORG UNIVERSITET
STUDENTERRAPPORT

10th Semester
AAU Energy
Pontoppidanstræde 111
9220 Aalborg Øst
http://www.en.aau.dk

Title:

Condition Monitoring of Hydraulic Actuator in Wind Turbine Pitch Systems: Investigation and EKF Implementation

Project Theme:

Master Thesis

Project Period:

From February 2023 to June 2023

Project Group:

Group MCE4 - 1021

Participants:

Niklas Enoch Andersen

Advisor:

Henrik C. Pedersen

Number of pages: 46

Synopsis:

Condition monitoring of wind turbines and their systems, is an area currently being researched and developed, due to the improvements it can provide for maintenance planning, fault detection and system performance. The focus of this study is to investigate condition monitoring methods, and to perform a theoretical study of a chosen method for condition monitoring of leakage faults in the hydraulic actuator of a wind turbine pitch system. A non-linear model will be developed as the basis for validation and comparisons, and a linear model will be developed for use in an extended Kalman filter. The extended Kalman filter will be developed for estimation of internal leakage of the hydraulic cylinder, and is tested against the non-linear model. Any errors that appear from the first test will be investigated and fixed for the extended Kalman filter to function correctly. The second test is run with success and the results are discussed and concluded upon, based on their usefulness in condition monitoring. The extended Kalman filter is deemed useful for condition monitoring of internal leakage in a hydraulic actuator, but is deemed in need of additional testing, and algorithms for more effective condition monitoring across a broader range of conditions.

Preface

The following project was completed by MCE4 - 1021 with the purpose of investigating condition monitoring methods for monitoring of leakage in the hydraulic actuator of a wind turbine pitch system, as well as investigation of implementation of one of the condition monitoring methods. The method chosen for the investigation is the extended Kalman filter, and development of a condition monitoring algorithm based on the filter

I would like to expresses my gratitude towards my project advisor Henrik C. Pedersen for his help.

The sources used in this report are marked in square brackets, e.g. [1]. If the source is placed before a period in a sentence, the source refers only to that sentence. If the source is placed outside the period, the source refers to the whole section.

Niklas

Niklas Enoch Andersen

nikand21@student.aau.dk

Resumé

Tilstandsovervågning af vindmøller og deres systemer, bliver undersøgt og forsket, da det er med til at udgøre markante forbedringer i planlægning af vedligeholdelse og bruges til fejlsporing af fejl før de sker, hvilket giver en reduktion i service og materialeomkostninger. Derudover er tilstandsovervågning med til at reducere driftnedlægningstider, på baggrund af bedre viden om systemets nuværende tilstand.

Denne rapport vil have fokus på undersøgelse af tilstandsovervågnings metoder og deres mulige brugbarhed i forhold til tilstandsovervågning af lækager i en hydraulisk cylinder som en del af en vindmølles hydrauliske vinkelstyringsystem. Forskellige metoder vil overvejes på baggrund af en state of the art undersøgelse, og en af metoderne vil blive udvalgt til implementering i en teoretisk undersøgelse af metodens brugbarhed og effektivitet i forhold til tilstandsovervågning. Metoden udvalgt til undersøgelse og implementering, er en metode baseret på et udvidet Kalman filter.

En ulineær model vil blive udviklet og valideret på baggrund af eksperimentelle data der er blevet målt fra en eksperimentel opsætning der er lavet til at simulere en vindmølles vinkelstyringssystem. Modellen udviser en generel dynamik der ligner dynamikken udvist af de eksperimentelle data, men med nogle afvigelser. Siden afvigelserne kan baseres på værdier der ikke helt passer til det eksperimentelle system, og siden dynamikken generelt stemmer overens, er den ulineære model dømt tilstrækkelig akkurat. Den efterligner et rigtigt vinkelstyringssystem godt nok til at den kan bruges til at teste på, men med nogle afvigelser som gør at der skal ske ændringer før tilstandsovervågningen pålideligt kan bruge på et rigtigt system.

Ud fra den ulineære model, vil der blive udviklet en lineær tilstandsrum model som skal bruges til det udvidede Kalman filter. Denne model bliver sammenlignet med den ulineære model for at finde potentielle uligheder mellem de to modeller. Sammenligningen viser at den lineære model efterligner den ulineære model godt, men med nogle få afvigelser som bliver set som ubetydelige når det skal bruge til et udvidet Kalman filter, da det kan kompensere for de små fejl. Efter den første test af filteret, bliver den lineære model undersøgt for fejl, da filteret begyndte at divergere kort efter starten af testen, hvilket resulterede i at filteret stoppede sine estimeringer. I undersøgelsen bliver nogle små afvigelser opdaget, hvilket kan forklares på baggrund af nogle forenklinger der blev introduceret som del af lineariseringen. Disse forenklinger bliver anset til at have en betydelig indflydelse på modellens udregninger, og bliver derfor indsat i den ulineære forudsigelse af systemets tilstande, hvilket giver en markant forbedring.

Det udvidede Kalman filter bliver udviklet til at estimere systemets tilstande, og til at estimere den interne lækage der sker i den hydrauliske cylinder. Dens ydeevne bliver testet i en sammenligning med den ulineære model. Den første test resulterer i en fejl da filterets kovarians matricer divergerer. Den anden test bliver kørt med forenklingerne inkluderet, og denne test ender i succes. Filteret estimerer trykkene godt, mens den estimerer vinklen og

vinkelhastigheden med nogle afvigelser og en mængde støj. Derudover estimerer filteret den interne lækage tilstrækkeligt, men med en del støj tilstede som kan obskure estimeringen.

Som konklusion, dømmes det udvidede Kalman filter til at være tilstrækkelig præcis i sine estimeringer, til at den kan bruges til tilstandsovervågning. Der skal dog udvikles mere med filtre eller tuning for at tilstandsovervågningen bliver mere tydelig og pålidelig. Derudover bør der udvikles algoritmer der kan bruge den estimerede lækage til at forudse hvornår lækagen bliver kritisk.

Table of Contents

1 Introduction

In response to the growing demand for green energy solutions, wind turbines have emerged as significant contributors, harnessing renewable energy at increasing rates. However, wind turbines are subject to various operational and environmental factors, such as high wind at sea, that can cause mechanical failures leading to significant downtime and maintenance costs. One of the difficulties for sea based wind turbines, is that they require more time and resources to maintain, due to the remote location and due to it being more difficult to reach than land based wind turbines. With cost being high, sending maintenance crews out for maintenance may be done less frequently. However, if crews are not sent out frequently enough, the wind turbines may end up being damaged due to wear, to the point where the wind turbine either produces much less power than intended, resulting in reduced income, or the wind turbine suffers permanent damage that may halt production completely and may be costly to repair. [1]

With this problem in mind, the introduction of condition monitoring (CM) into the wind turbine system could prove useful in predicting and detecting faults in the system, before any serious damage or significant performance loss. Condition monitoring involves the use of various sensors and data analysis tools to continuously monitor the health of wind turbine components. One of the components that may experience faults is the hydraulic cylinder which actuates the pitch. The cylinder may not fail as frequently as other components [1], but it may wear down over time, resulting in lower efficiency, which has a significant influence on the overall system efficiency. By identifying and addressing problems in the pitch cylinder early, condition monitoring can help optimize the maintenance schedules, reduce operational costs and increase the lifespan of the cylinder and by extension, the wind turbine. [2]

This report will present as study on the various techniques and methods used in condition monitoring of wind turbines. Additionally, a method will be chosen for a theoretical study of its application on a wind turbine pitch system. The results of this study will be analysed for their usefulness in tackling the problem of pitch system cylinder failures.

1.1 Problem Statement

The main objective is to investigate whether a chosen condition monitoring algorithm can effectively detect and predict leakage faults in the hydraulic cylinder of a wind turbine pitch system. Developing and implementing condition monitoring for a wind turbine requires general knowledge about different condition monitoring methods, so that all options are considered. As such, the state of the art of condition monitoring methods will need to be investigated. Apart from this, the goal of the condition monitoring is to detect changes in the system relating to leakage in the hydraulic cylinder. It should be able to detect when leakage occurs, and to some degree predict when internal leakage is significantly lowering the pitch system performance. The intention is for the condition monitoring to be able to warn about leakage faults, whether incipient or not.

A general description of the objective can be formulated as in the following statement:

Investigate condition monitoring methods, and the effectiveness of a chosen condition monitoring method for leakage fault detection and prediction, when implemented on the actuating hydraulic cylinder of a wind turbine pitch system

As this is an investigation of the effectiveness of a chosen condition monitoring method, the final results can range from very effective to unusable. Many factors can have an influence on this, and it should be noted that any result from this investigation will only apply to the investigated system or very similar systems. The objective brings an additional sub-objective that is required to complete the main objective.

It will be necessary to design a dynamic model of the hydraulic wind turbine pitch system, as this will be useful for testing and may be required by some condition monitoring methods. A dynamic model will also allow for the development of control for the system.

1.2 Limitations

Given that this investigation may be very broad, and can be completed in many different ways, it is necessary to state the limitations that are present due to circumstances and the limitations that are applied for the sake of limiting the scope of the investigation.

One limitation is the limited availability of experimental setups and equipment. Because of this, the testing of the algorithm will be done exclusively on the dynamic nonlinear model, making the final results completely theoretical. Additionally, the final results will depend on the accuracy of the model, and will be affected by any simplifications that may be included as well. Most values used in the model will originate from data provided for the project.

A second limitation is present somewhat due to the first limitation. Since there will be no experimental setup, the testing will have to rely on a set of previously measured values as input into the dynamic model. This will limit the testing of the model and algorithm to the given data, simple manually designed inputs, and potentially randomised signals based on the aforementioned data. This should still give a decent idea of the model accuracy and algorithm effectiveness, but may limit them somewhat.

The state of the art will be investigated, but only one condition monitoring method will be chosen for implementation. This is to limit the overall scope of the objective.

1.3 State of the Art

Condition monitoring of wind turbines is important for the effectiveness and reliability of wind turbines, and many condition monitoring methods have been developed and used for wind turbines. Because of this, the state of the art has been investigated for the purpose of finding a fitting condition monitoring method for the pitch system cylinder. Different condition monitoring methods were considered. The methods deemed most fitting is included in this section and evaluated for use on the cylinder leakage.

1.3.1 Acoustic Emission

Acoustic emission sensors can be mounted on critical areas for precise acoustic measurements. This is useful for detecting faults such as structural damage and fatigue, both of which can be useful for condition monitoring of cylinder leakages. A downside of this method is the necessity of acquisition and application of acoustic sensors, which can be expensive and may require changes in the wind turbine design or layout as there may not be room for the sensors, depending on the turbine. [1]

1.3.2 Thermography analysis

Thermography analysis is a useful condition monitoring method that can be used in many cases. Using IR sensors or cameras, it is possible to detect a variety of faults through the changes in temperature caused by said faults. This may be useful for condition monitoring of the internal cylinder leakage, as internal leakage may indicate the seal deteriorating due to fatigue, which will increase friction, causing more heat in the cylinder. The downsides for this method include the precision depending on the resolution of the IR equipment, and that the method is not well suited for early warnings, as temperature develops slowly. [1]

1.3.3 Model based methods

Model based condition monitoring methods present a way of implementing condition monitoring without it being necessary to add additional sensors to the system. These methods use mathematical models to simulate the dynamic behaviour of the system during optimal operation. Using the output of the simulations, the difference between the actual system and the simulation can be obtained. One way to implement model based condition monitoring, is through the use of observers. Model based methods are highly dependant on the design of the model, which may be challenging depending on the system. [3, 4]

1.3.4 Vibration analysis

Vibration analysis could be useful for condition monitoring of leakage in the cylinder since any leakage, internal and external, will likely generate some amount of vibrations that can be detected by measuring equipment. This method requires sensors to be installed, such as position transducers, velocity sensors and accelerometers, which also introduces the potential problem of available space in the turbine. The method is generally well know and efficient when introduced to a variety of wind turbine components, but it is not known to be useful for cylinder leakage detection. Additionally, vibration analysis may not be effective in detecting incipient faults in the system, making it more of a reactive condition monitoring method. [1]

Each of the condition monitoring methods have their positives and negatives, and each of them could potentially be used for the detection of leakage in the cylinder. However, most of the methods mentioned, require an amount of measuring equipment to be installed in the wind turbine, either through attachment to a surface, or through placement within a component or structure. The latter would not be ideal for hydraulic systems as they could introduce new point of potential leakage, or they may weaken some parts in order to accommodate them. Avoiding this could necessitate new components specifically made for this design, adding to the cost of introducing the sensor. Using surface mounted sensors may be less intrusive, but can still make changes necessary due to potentially limited space. A second point to consider relating to the condition monitoring methods, is prediction capability. Since faults in the cylinder related to leakage may result in oil being spilled inside the wind turbine, it is best avoided entirely, as this could lessen the work needed by maintenance crews, as well as the cost of maintenance. Cylinder leakage also results in deteriorating performance of the pitch system, which makes it preferable for a condition monitoring system to be capable of detecting incipient faults. This would also allow for maintenance scheduling, as the condition monitoring system would be able to propose good cost effective maintenance time frames.

With these considerations in mind, the condition monitoring method chosen for the cylinder leakage detection is the model based method. This method can require pressure values, which may be measured or calculated, as the model can potentially be designed to function with a variety of measurements. The model would as such, preferably be designed to use the measurements that are available at the turbines current design. Furthermore, the model based method could be able to detect incipient faults, depending on the quality of the model design.

Model based methods is a category of condition monitoring methods that, as the name suggests, are based upon a model of the system. Because of this, a specific method will have to be chosen for the case of cylinder leakage. Given that cylinder leakage is difficult to precisely model, it would be advantageous to make use of the extended Kalman filter (EKF). The extended Kalman filter allows for the estimation of system values that are not part of the original model, and is therefore useful for estimating cylinder leakage. Apart from this, the extended Kalman filter is also useful as an observer, and can be used to calculate residuals, which can further enhance the condition monitoring algorithm. [4]

System Model 2

In order to implement any model based CM method, it is essential to have an understanding of the system dynamics under normal operation without faults. This is necessary for development of a dynamic model of the system, which of course is necessary for model based CM approaches, such as EKF. This chapter will describe how the system model is developed, and is divided into hydraulic and mechanical parts.

2.1 Hydraulic Model

The hydraulic system of the pitch system can be somewhat simplified for the purposes of condition monitoring of the cylinder. Since the cylinder is the focus, any accumulators that may be part of a pitch system, are neglected, and the supply pressure provided by the supply circuit is assumed constant for simplicity. The hydraulic system considered in this case consists of a cylinder, a proportional valve, supply and tank ports, as well as pressure measurement gauges. The hydraulic system is depicted in figure 2.1. [2]

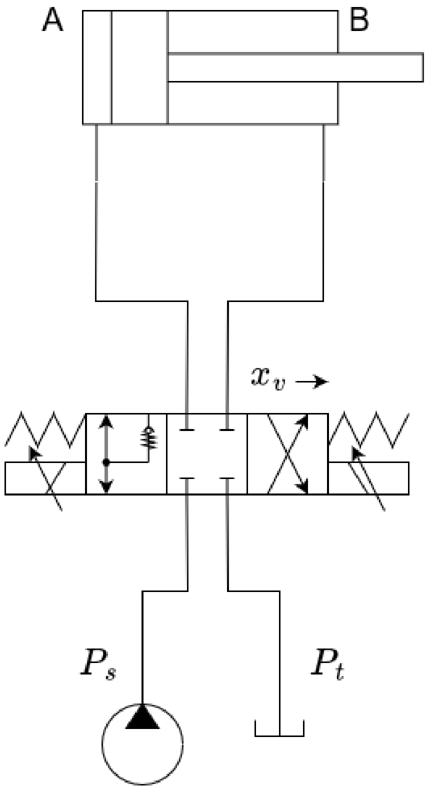

Figure 2.1. *Hydraulic system diagram.*

The two chamber volumes of the cylinder are denoted A and B on the sketch, and will be referred to as A- and B-chambers. The supply and tank lines are connected to a proportional servo valve, with a design that makes it normally closed. The proportional valve is then connected to the cylinder on the opposite side. When the valve position x_{pv} is negative, the lines are inverted though the valve, and when x_{pv} is positive, only the supply pressure is used, supplying one output line, while the other line has a check valve attached, meaning it only allows flow coming from the cylinder. This results in the B-chamber always being pushed to have a slightly higher pressure than the A-chamber when x_{pv} is positive. The proportional valve is also illustrated in figure 2.1 on the preceding page.

The cylinder chambers are modelled using continuity equations. The initial equation is shown in equation (2.1). [5]

$$Q_{in} - Q_{out} = \dot{V} + \frac{V}{\beta}\dot{p} \tag{2.1}$$

This equation is then reformulated to isolate the pressure change, giving the equation shown in equation (2.2).

$$\dot{p} = \frac{\beta}{V} \cdot (Q_{in} - Q_{out} + \dot{V}) \tag{2.2}$$

Where V is the volume, $\dot{V}$ is the volume change, $\dot{P}$ is the pressure change, β is the bulk modulus of the fluid-air mixture, Q_{in} is the flow into the cylinder chamber and Q_{out} is the flow out of the chamber. The pressure value acquired after taking the integral of the pressure change, is used as a feedback in the model. This is essential for the calculation of the orifice equations of the proportional valve, and for estimation of the bulk modulus. The proportional valve orifice equations can be seen in equation (2.3) and equation (2.4). [5]

$$Q_A = \begin{cases} C_{vv} \cdot \sqrt{|P_A - P_t|} \cdot sign(P_A - P_t), & x_v < 0 \\ C_{vv} \cdot \sqrt{|P_s - P_A|} \cdot sign(P_s - P_A), & x_v > 0 \\ 0, & x_v = 0 \end{cases} \tag{2.3}$$

$$Q_B = \begin{cases} C_{vv} \cdot \sqrt{|P_s - P_B|} \cdot sign(P_s - P_B), & x_v < 0 \\ Kcv \cdot (P_B - P_s - P_c), & x_v > 0 \wedge P_B > P_s - P_c \\ 0, & x_v = 0 \vee (x_v > 0 \wedge P_B < P_s - P_c) \end{cases} \tag{2.4}$$

$$C_v = \frac{Q_{nom}}{\sqrt{P_{nom}}} \tag{2.5}$$

Where Q_i is the flow through the valve running in connection to the i chamber, P_i denotes pressure of chamber i and Cv is a valve coefficient calculated from nominal flow and pressure and seen in equation (2.5). It can be seen that the orifice equation on the B side is dependent on the crack pressure of the internal check valve and the B side pressure.

The bulk modulus used in the continuity equations is estimated using equation (2.6). [5]

$$\beta = \frac{(1-\alpha)\cdot \exp\left\{\frac{P_0 - P}{\beta_0}\right\} + \alpha \cdot (\frac{P_0}{P})^{\frac{1}{n}}}{\frac{1-\alpha}{\beta_0}\cdot \exp\left\{\frac{P_0 - P}{\beta_0}\right\} + \frac{\alpha}{n_0}\cdot (\frac{P_0}{P})^{\frac{n+1}{n}}} \tag{2.6}$$

Where P_0 is the initial pressure, β_0 is the initial constant stiffness of the fluid, α is the ratio of air volume to the total volumes at atmospheric pressure and n is the poly tropic index number, which for this system is set to 1,4 denoting an adiabatic process. This estimation is used with the assumption of the oil stiffness being constant during operation of the pitch system.

2.2 Mechanical Connection Model

The mechanical connection between the hydraulic cylinder and the wing pitch bearing can be modelled using kinematic and dynamic equations, and is illustrated in the sketch in figure 2.2. The kinematic relation between the cylinder position and the pitch of the blade is modelled using the law of cosines as seen in equation (2.7).

$$x_{cyl} = \sqrt{L_{AE}^2 + L_{BE}^2 - 2L_{AE}L_{BE}cos(\phi_p + \phi_0)} - L_{AB0} \tag{2.7}$$

Where x_{xcyl} is the cylinder position, L_{xy} is the length between x and y, ϕ is the angle between L_{AC} and the pitching angle ϕ_p, which is defined as the angle of the blade relative to the minimum angle. The minimum angle ϕ_0 is defined as the difference between ϕ and ϕ_p. L_{AB0} is the cylinder dead length. A sketch showing the mechanical connections is seen in figure 2.2 [6].

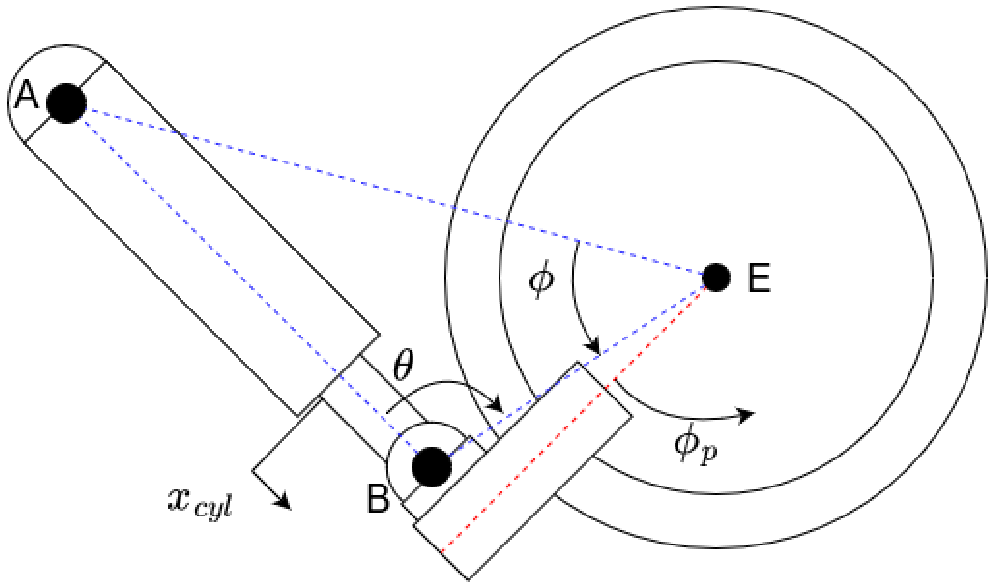

Figure 2.2. *Mechanical connection sketch.*

The θ angle is related to the cylinder position x_{cyl} as shown in equation (2.8).

$$\theta = acos(\frac{L_{AB0} + x_{cyl}^2 - L_{AE}^2 + L_{BE}^2}{2_{BE} \cdot (L_{AB0} + x_{cyl})}) \tag{2.8}$$

As seen in figure 2.2, the system consist of a cylinder and a disc bearing that rotate together. The movement of the system can be described using Newtons second law for rotation seen in equation (2.9).

$$\tau_{eq} = J_{eq} \cdot \ddot{\phi}_p = \tau_{cyl} - \tau_{fric} - \tau_{wing} \tag{2.9}$$

This equation shows that the angular acceleration is dependant on the equivalent inertia of the system J_{eq}, the applied cylinder torque τ_{cyl}, the friction torque τ_{fric} and the load torque applied by the wind τ_{wing}. The inertia and torques are described by equations (2.10) to (2.13).

$$J_{eq} = \left(\frac{\partial x_{cyl}}{\partial \phi_p}\right)^2 m_{pist} + J_w \tag{2.10}$$

The equivalent inertia is calculated from the cylinder piston inertia and the pitch bearing mass moment of inertia. The cylinder piston moment of inertia is modelled using the equation for moment of inertia of a single point mass: $I = m \cdot r^2$, as an approximation. The mass of the equation is the piston mass, denoted m_{pist}. The length in the equation changes throughout operation, and can be described as the partial derivative of x_{cyl} with respect to ϕ_p.

The pitch bearing mass moment of inertia is a supplied parameter, and does not need to be calculated.

$$\tau_{cyl} = F_{cyl} \cdot L_{BE} \cdot sin(\theta) \tag{2.11}$$

The cylinder torque is calculated from the torque equation with the cylinder force inserted. The cylinder force is calculated from the difference between the forces applied by the pressures of each cylinder chamber, as shown in equation (2.12).

$$F_{cyl} = P_A \cdot A_A - P_B \cdot A_B \tag{2.12}$$

$$\tau_{fric} = tanh(\dot{x}_{cyl}) \cdot F_{stat} + F_{vis} \cdot \dot{x}_{cyl} \tag{2.13}$$

The friction torque is calculated based on the friction forces. The static friction is based on the direction in which the cylinder piston is moving, and the viscous friction is based on the velocity of the cylinder piston. The friction force coefficients: F_{stat} and F_{vis} are supplied parameters.

2.3 Non-linear Model Validation

To ensure that the non-linear model behaves like the pitch system of an actual wind turbine, the non-linear model will have to be validated and compared with experimental data. For the model to be sufficiently validated, the model should be able to follow the same pattern as the experimental data, while not deviating to an overly significant degree. The nonlinear model is controlled by a simple PI controller, tuned to follow a given trajectory with minimal deviation from the reference.

Experimental data from an actual turbine was not available for this validation. However, data acquired from an experimental setup emulating an actual wind turbine pitch system was made available, providing data resembling the behaviour of a wind turbine. This experimental setup uses a load cylinder to emulate the load that would be applied by the wind in a real case. The data available from an experiment on this setup runs for 11 seconds, and includes data from the pitch value, the load cylinder pressures and the available supply pressure. The load cylinder pressures are used to calculate the load torque applied to the system, in the same way that the applied pitching cylinder torque is calculated, shown in equations (2.11) and (2.12) on the facing page. Graphs of the proportional valve data, the supply pressure data and the load torque data, can be seen in figures 2.3 to 2.5 on pages 11–12.

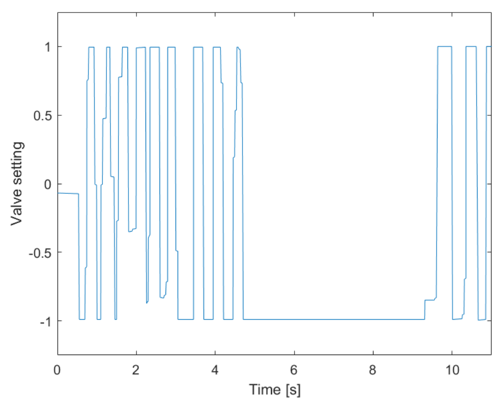

Figure 2.3. *Proportional valve setting.*

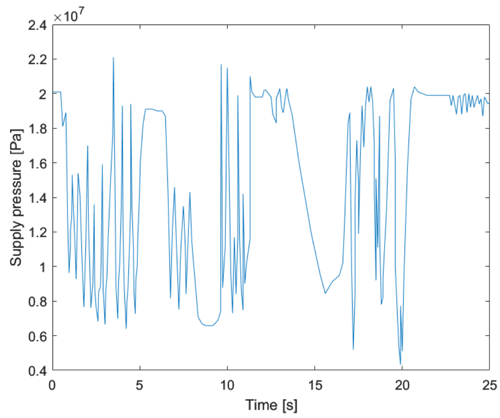

Figure 2.4. *Experiment supply pressure.*

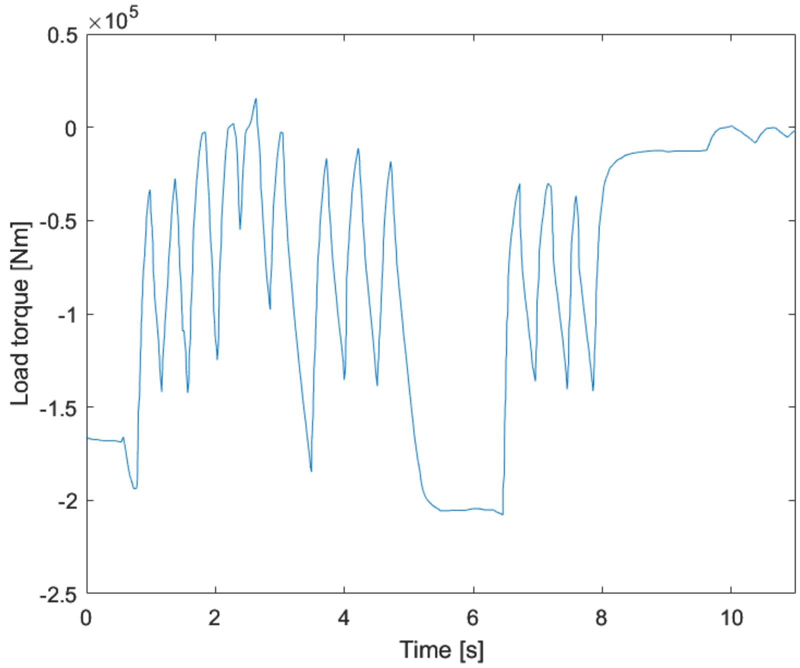

Figure 2.5. *Experiment load torque.*

The resulting experiment pitch is compared with the pitch result acquired from the nonlinear model, and the pressures of the pitch cylinder are acquired from the nonlinear model. Graphs showing the comparison and the pressures can be seen in figures 2.6 and 2.7 on the current page and on the facing page.

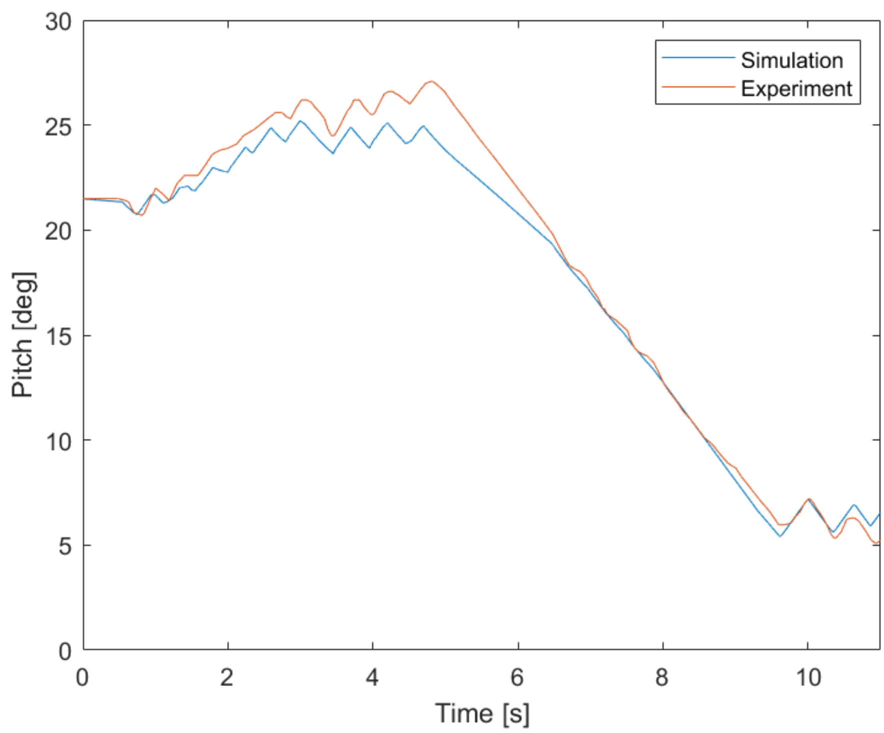

Figure 2.6. *Pitch comparison.*

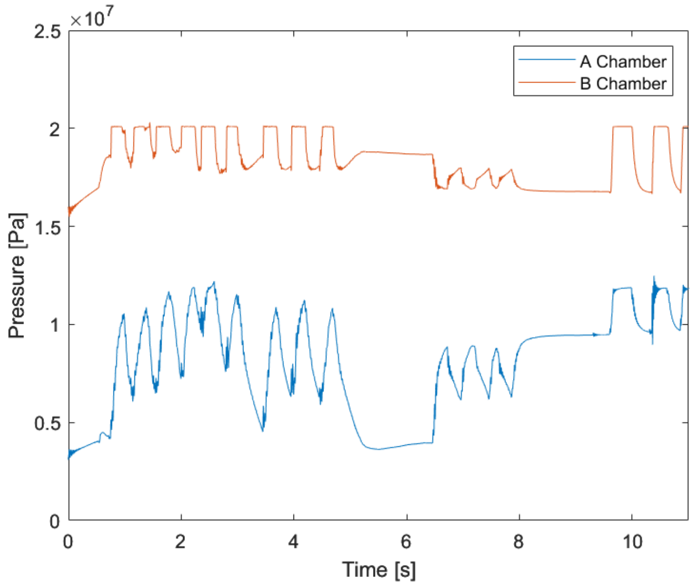

Figure 2.7. *Nonlinear model pressures.*

It can be seen in figure 2.6 on the preceding page that the pitch result of the simulation follows the same pattern as the experiment pitch, while deviating from the precise value of the experiment pitch. Because of this, the nonlinear model is not very accurate, but is able to simulate general wind turbine behaviour. Since wind turbine behaviour is the main purpose of the nonlinear model, and since the accuracy of the model is somewhat accurate, the nonlinear model is deemed sufficiently validated.

The pressure results from the nonlinear model seen in figure 2.7, show that the B-chamber pressure remains varying around and at the supply pressure, which stays close to 200 bar. This shows the dynamics of the check valve which are applied whenever the proportional valve is in a positive position. The A-chamber pressure remains around half the value of the B-chamber pressure, showing the balance between forces applied by the pressures over their respective cylinder areas.

This nonlinear model will function as the base system of which the linear model and the Kalman filter results will be compared to.

2.4 State Space Model

Design of an extended Kalman filter, requires a state space model of the system, as the filter uses the state space matrices as part of both the prediction and correction parts. As such, the system needs to be linearised to enable the use of linear control theory, and allow for the state space model to be constructed. Linearisation is performed using the first order Taylor approximation, as shown in equation (2.14).

$$F_L = F_{nonL}(X_L) + \left.\frac{\partial F_{nonL}(X)}{\partial X}\right|_{X_L} (X - X_L) \tag{2.14}$$

Where X is the state vector as seen in equation (2.15). The state include the two cylinder chamber pressures, as well as the pitch angle and the pitch angular velocity.

$$X = \begin{bmatrix} P_A \\ P_B \\ \phi_p \\ \dot{\phi}_p \end{bmatrix} \tag{2.15}$$

The linearisation is used to approximate linear expressions of the dynamic equations describing the system states. The linearisation point vector X_L denotes the points at which the linear approximations are evaluated. F_L is the linear approximation of the corresponding nonlinear dynamic equation F_{nonL}.

The nonlinear dynamic system equations are developed using the equations shown in previous sections, namely: equations (2.2) and (2.9) on page 7 and on page 9. The continuity equation will be used for both the A and B-chamber pressure changes, and variables corresponding to these chambers are named accordingly. All of the equations used to calculate the values of F_{nonL} can be found in equations (2.16) to (2.18).

$$\begin{aligned} \dot{P}_{Af} &= \frac{\beta}{V_{A0} + x_{cyl} A_a}(Q_A - A_a \dot{x}_{cyl}) \\ Q_A &= \begin{cases} \frac{Q_{nom}}{\sqrt{P_{nom}}} x_v \sqrt{|P_A - P_t| \cdot sign(P_A - P_t)}, & x_v < 0 \\ \frac{Q_{nom}}{\sqrt{P_{nom}}} x_v \sqrt{|P_s - P_A| \cdot sign(P_s - P_A)}, & x_v > 0 \end{cases} \end{aligned} \tag{2.16}$$

$$\begin{aligned} \dot{P}_{Bf} &= \frac{\beta}{V_{B0} + x_{cyl} A_b}(A_b \dot{x}_{cyl} - Q_B) \\ Q_B &= \begin{cases} \frac{Q_{nom}}{\sqrt{P_{nom}}} x_v \sqrt{|P_s - P_B| \cdot sign(P_s - P_B)}, & x_v < 0 \\ Kcv \cdot (P_B - P_s - P_c), & x_v > 0 \end{cases} \end{aligned} \tag{2.17}$$

$$\ddot{\phi}_{pf} = \frac{1}{\frac{\partial x_{cyl}}{\partial \phi_p}^2 m_{pis} + J_b}\left(\frac{\partial x_{cyl}}{\partial \phi_p}\frac{\partial^2 x_{cyl}}{\partial \phi_p{}^2}\dot{\phi}_p + M_{cyl} + M_{Pitch}\right) \tag{2.18}$$

2.4.1 Simplifications

Some parts of the system model can be simplified, resulting in a less complex state space model. Some of these simplifications will likely have a negative effect on the accuracy of the linear model, while making the necessary calculations significantly simpler. The first simplification is the replacement of the cylinder piston position equation with a linear function based on the dynamic behaviour of the piston position. Looking at the piston position change in relation to the pitch angle shown in figure 2.8, it can be seen that a large part of the movement is somewhat linear.

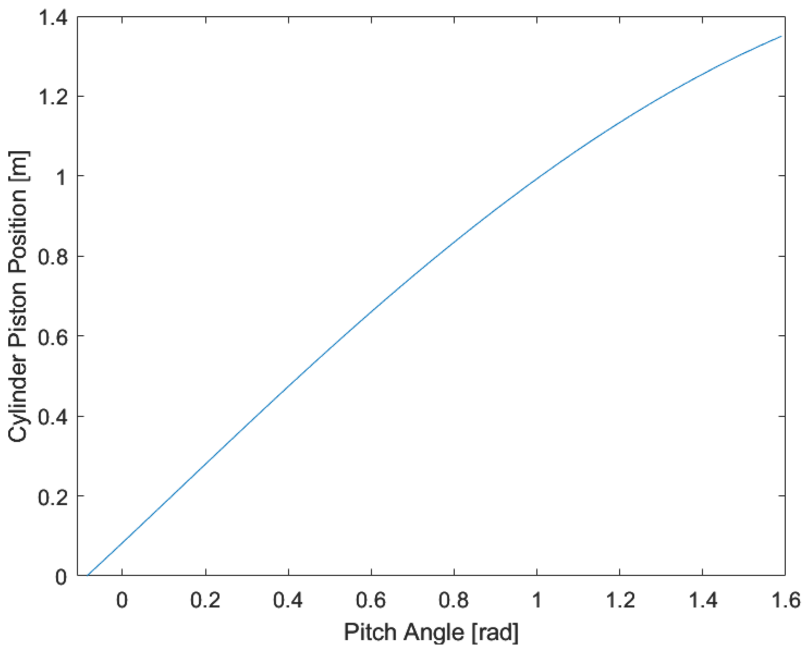

Figure 2.8. *Cylinder position as a function of pitch angle.*

From the data shown in the graph, it is possible to construct a simple linear function that is able to follow the nonlinear behaviour with only small amounts of deviation at the majority of the cylinder range. Simply multiplying the slope of the nonlinear function when the pitch angle is low, with the pitch as shown in equation (2.19) on the next page, gives a somewhat similar linear function. The functions are compared in figure 2.9 on the following page.

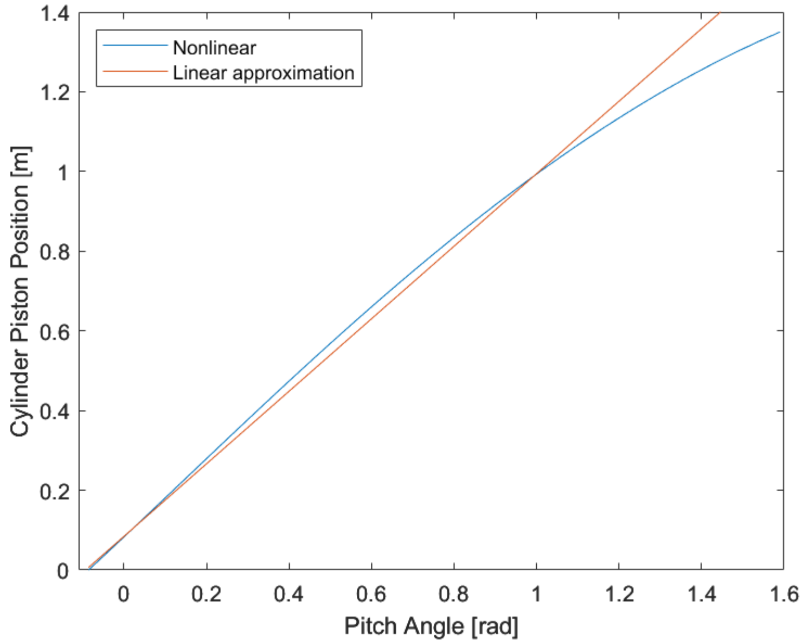

Figure 2.9. *Linear and nonlinear function comparison.*

$$x_{cyl} = 0.9101\phi_p + 0.08426 \tag{2.19}$$

It can be seen that the functions generally follow each other in output through the pitch angles, except when the pitch angle gets near the maximum. Since the pitch will rarely move to angles that high, the linear function can work as a simplification of the piston position.

A second simplification involves the dynamic behaviour of the proportional valve. Since the behaviour of the rest of the system is comparatively slower than the valve, the dynamic behaviour could be neglected. Instead, the valve position is assumed to move to the desired position instantly. As such, the control valve dynamics are omitted from the linear model, and the input is directly applied to the orifice equations.

Additionally, the bulk modulus can also be simplified. The dynamic bulk modulus equation shown in equation (2.6) on page 8 develops in a nonlinear fashion, but the dynamics quickly cease as the pressure increases. Assuming the system runs with high pressures throughout operation, the dynamic bulk modulus equation can be replaced by a constant bulk modulus value of 16000 bar which is the maximum bulk modulus provided by the dynamic equation. This will reduce the accuracy of the state space model when running at low pressures. A last simplification can be implemented in the continuity equations. Assuming that the pitch will only perform small changes, and that it will remain close to the starting point at zero degrees, will make it possible to omit the change in cylinder chamber volume. This will result in a simpler model, that is less accurate the more the pitch moves away from the starting 0 degrees. This assumption is based on the fact that the pitch should only move slightly to counteract torque applied by the wind, and should preferably stay close to zero degrees for the wing to gain the maximum amount of energy from the wind.

2.4.2 Linearization

Linearizing the nonlinear system for use in a state space model, can be done through partial differentiation as shown in equation (2.14) on page 14. This means that the nonlinear differential equations describing the nonlinear system will have to be differentiated to every state and every input. The resulting partial derivatives can then be used to construct the system matrix, input matrix and measurement matrix of the state space system, as shown in equations (2.20) to (2.22).

$$A = \frac{\partial F_{nonL}}{\partial X} \tag{2.20}$$

$$B = \frac{\partial F_{nonL}}{\partial u} \tag{2.21}$$

$$C = \frac{\partial H}{\partial X} \tag{2.22}$$

Where u is the input to the system, F_{nonL} is a vector of the dynamic system equations used to calculate $\dot{X}$, and H is the output vector, which denotes the states that are measured or output. The different differential equations that will be used for linearization are calculated throughout the rest of this section. The derivatives will be shown without being evaluated at the linearization point, as the extended Kalman filter will need to linearize to changing linearization points.

The flow equations change depending on the proportional valve position, and because of this, the derivatives of the flow equations will be separated depending on the valve position. The derivatives of the flows when $x_v < 0$ are shown in equations (2.23) to (2.28).

$$\frac{\partial Q_A}{\partial P_A} = \frac{C_v \cdot x_v}{2\sqrt{P_A - P_t}} \tag{2.23}$$

$$\frac{\partial Q_B}{\partial P_A} = 0 \tag{2.24}$$

$$\frac{\partial Q_A}{\partial P_B} = 0 \tag{2.25}$$

$$\frac{\partial Q_B}{\partial P_B} = -\frac{C_v \cdot x_v}{2\sqrt{P_s - P_B}} \tag{2.26}$$

$$\frac{\partial Q_A}{\partial x_v} = C_v \cdot \sqrt{P_A - P_t} \tag{2.27}$$

$$\frac{\partial Q_B}{\partial x_v} = C_v \cdot \sqrt{P_s - P_B} \tag{2.28}$$

The derivatives of the continuity equations are shown in equations (2.29) to (2.38) on the next page.

$$\frac{\partial \dot{P}_A}{\partial P_A} = \frac{\beta \cdot \frac{\partial Q_A}{\partial P_A}}{V_{A0}} \tag{2.29}$$

$$\frac{\partial \dot{P}_B}{\partial P_A} = 0 \tag{2.30}$$

$$\frac{\partial \dot{P}_A}{\partial P_B} = 0 \tag{2.31}$$

$$\frac{\partial \dot{P}_B}{\partial P_B} = -\frac{\beta \cdot \frac{\partial Q_B}{\partial P_B}}{V_{A0}} \tag{2.32}$$

$$\frac{\partial \dot{P}_A}{\partial \phi} = -\frac{A_A \cdot \beta \cdot \frac{\partial \dot{x}}{\partial \phi_p}}{V_{A0}} \tag{2.33}$$

$$\frac{\partial \dot{P}_B}{\partial \phi} = \frac{A_B \cdot \beta \cdot \frac{\partial \dot{x}}{\partial \phi_p}}{V_{B0}} \tag{2.34}$$

$$\frac{\partial \dot{P}_A}{\partial \dot{\phi}} = -\frac{A_A \cdot \beta \cdot \frac{\partial \dot{x}_{cyl}}{\partial \dot{\phi}}}{V_{A0}} \tag{2.35}$$

$$\frac{\partial \dot{P}_B}{\partial \dot{\phi}} = \frac{A_B \cdot \beta \cdot \frac{\partial \dot{x}_{cyl}}{\partial \dot{\phi}}}{V_{B0}} \tag{2.36}$$

$$\frac{\partial \dot{P}_A}{\partial x_v} = \frac{\beta \cdot \frac{\partial Q_A}{\partial x_v}}{V_{A0}} \tag{2.37}$$

$$\frac{\partial \dot{P}_B}{\partial x_v} = -\frac{\beta \cdot \frac{\partial Q_B}{\partial x_v}}{V_{B0}} \tag{2.38}$$

Finally, the derivatives of the angular acceleration acquired from equation (2.9) on page 9 can be seen in equations (2.39) to (2.43).

$$\frac{\partial \ddot{\phi}}{\partial P_A} = \frac{A_{ABE}(\theta)}{(\frac{\partial x_{cyl}}{\partial \phi})^2_{pist} + J_w} \tag{2.39}$$

$$\frac{\partial \ddot{\phi}}{\partial P_B} = -\frac{A_{BBE}(\theta)}{(\frac{\partial x_{cyl}}{\partial \phi})^2_{pist} + J_w} \tag{2.40}$$

$$\frac{\partial \ddot{\phi}}{\partial x_v} = 0 \tag{2.41}$$

$$\frac{\partial \ddot{\phi}}{\partial \phi} = \frac{\frac{\partial M_{cyl}}{\partial \phi_p} - \frac{\partial T_{fric}}{\partial \phi_p}}{(\frac{\partial x_{cyl}}{\partial \phi})^2_{pist} + J_w} \tag{2.42}$$

$$\frac{\partial \ddot{\phi}}{\partial \dot{\phi}} = -\frac{\frac{\partial T_{fric}}{\partial \dot{\phi}_p}}{(\frac{\partial x_{cyl}}{\partial \phi})^2_{pist} + J_w} \tag{2.43}$$

2.4.3 State Space Representation

With the partial derivatives calculated, they can be inserted into the state space representation, shown in equation (2.44). Inserting linearization points into the model will result in the linearised state space model of the system.

$$\begin{aligned}\dot{X} &= AX + Bu \\ y &= CX\end{aligned} \tag{2.44}$$

The values of the state matrices are calculated throughout this section from the derivatives. As mentioned previously, the flow equations change depending on the proportional valve position, meaning that two state space models are developed from the linearizations. Inserting the derivatives into the continuity equations and the angular acceleration equation, results in linear approximations of said equations, excluding the linearization points. The linear equations are shown in equations (2.45) to (2.47).

$$\Delta\dot{P}_{A,ss} = \frac{\partial \dot{P}_A}{\partial P_A} \cdot \Delta P_A + \frac{\partial \dot{P}_A}{\partial \phi} \cdot \Delta\phi + \frac{\partial \dot{P}_A}{\partial \dot{\phi}} \cdot \Delta\dot{\phi} + \frac{\partial \dot{P}_A}{\partial x_v} \cdot \Delta x_v \tag{2.45}$$

$$\Delta\dot{P}_{B,ss} = \frac{\partial \dot{P}_B}{\partial P_B} \cdot \Delta P_B + \frac{\partial \dot{P}_B}{\partial \phi} \cdot \Delta\phi + \frac{\partial \dot{P}_B}{\partial \dot{\phi}} \cdot \Delta\dot{\phi} + \frac{\partial \dot{P}_B}{\partial x_v} \cdot \Delta x_v \tag{2.46}$$

$$\Delta\ddot{\phi}_{ss} = \frac{\partial \ddot{\phi}}{\partial P_A} \cdot \Delta P_A + \frac{\partial \ddot{\phi}}{\partial P_B} \cdot \Delta P_B + \frac{\partial \ddot{\phi}}{\partial \phi} \cdot \Delta\phi + \frac{\partial \ddot{\phi}}{\partial \dot{\phi}} \cdot \Delta\dot{\phi} \tag{2.47}$$

These equations can be put into state space form, resulting in equation (2.51), where the differential equations and their results are replaced with coefficients as shown in equations (2.48) to (2.50).

$$\Delta\dot{P}_{A,ss} = a_1 \cdot \Delta P_A + a_2 \cdot \Delta\phi + a_3 \cdot \Delta\dot{\phi} + b_1 \cdot \Delta x_v \tag{2.48}$$

$$\Delta\dot{P}_{B,ss} = a_4 \cdot \Delta P_B + a_5 \cdot \Delta\phi + a_6 \cdot \Delta\dot{\phi} + b_2 \cdot \Delta x_v \tag{2.49}$$

$$\Delta\ddot{\phi}_{ss} = a_7 \cdot \Delta P_A + a_8 \cdot \Delta P_B + a_9 \cdot \Delta\phi + a_{10} \cdot \Delta\dot{\phi} \tag{2.50}$$

$$\begin{aligned}\begin{bmatrix}\dot{P}_{Af} \\ \dot{P}_{Bf} \\ \dot{\phi}_{pf} \\ \ddot{\phi}_{pf}\end{bmatrix} &= \begin{bmatrix} a_1 & 0 & a_2 & a_3 \\ 0 & a_4 & a_5 & a_6 \\ 0 & 0 & 0 & 1 \\ a_7 & a_8 & a_9 & a_{10}\end{bmatrix}\begin{bmatrix}P_A \\ P_B \\ \phi_p \\ \dot{\phi}_p\end{bmatrix} + \begin{bmatrix}b_1 \\ b_2 \\ 0 \\ 0\end{bmatrix} x_v \\ y &= C\begin{bmatrix}P_A \\ P_B \\ \phi_p \\ \dot{\phi}_p\end{bmatrix}\end{aligned} \tag{2.51}$$

The hydraulic system dynamics are dependant on the proportional valve spool position, as shown in equations (2.3) and (2.4) on page 7. Because of this, it would be necessary to create two state space models, each representing the dynamics of the system at either positive or negative valve spool positions, if a very precise linear model is needed. However, since the linear state space models will be used for a Kalman filter, the models may not need to be exceedingly accurate, as the filter will be able to correct some amount of inaccuracy. However, if the linear model is significantly inaccurate, or if the non-linear system is significantly non-linear, the Kalman filter may not be able to perform as intended. As such, it is necessary to validate and test the linear model, as it has a significant influence on the Kalman filter performance.

2.4.4 Linear Pitch Extension Model

The model that has been developed to this point, is modeled for the case where the hydraulic piston is meant to shorten in length to reduce blade pitch. If the system moves in the opposite direction, the proportional valve will have to move to positive position values, which in turn, will change the effective dynamics of the system. Because of this, it is necessary to develop an additional linear model that takes the new dynamics into account. The only changes that are introduced to the system dynamics, is a change in how the flows are calculated. Since the direction of flow is changed for the A-port, the calculation of the flow is based on how the new pressures interact as shown in equation (2.52).

The B-flow calculation is significantly changed, as instead of being connected to the tank, it is instead connected to the supply pressure together with the pressure of A-chamber. However this is only the case when the pressure of the B-chamber becomes larger than the supply pressure and crack pressure of the check valve. Modeling this accurately will require another linear model, so that both states of the check valve are modelled. However, keeping in mind that the B-chamber volume of the cylinder will be continuously decreased during extension, the pressure in the B-chamber will be pushed above the required pressure for the check valve to open. This results in a loop that keeps the B-chamber pressure more or less constant at supply pressure throughout the piston extension. Because of this, the B-chamber pressure can be assumed constant, and equal to the supply pressure, denoted in equation (2.53).

$$Q_A = \frac{Q_{nom}}{\sqrt{P_{nom}}} x_v \sqrt{|P_s - P_A|} \cdot sign(P_s - P_A) \tag{2.52}$$

$$P_B \approx P_s \tag{2.53}$$

This simplification can make the model less accurate, as supply pressures are not constant in reality, and the B-chamber pressure will in a real case fluctuate around the supply pressure. With this in mind, the partial derivatives needed for the second linear model, developed in the case where $x_v > 0$, are shown in equations (2.54) and (2.55).

$$\frac{\partial Q_A}{\partial P_A} = \frac{Q_{nom}}{\sqrt{P_{nom}}} \cdot \frac{x_v}{2 \cdot \sqrt{|P_s - P_A|}} \tag{2.54}$$

$$\frac{\partial Q_A}{\partial x_v} = \frac{Q_{nom}}{\sqrt{P_{nom}}} \cdot \sqrt{|P_s - P_A|} \tag{2.55}$$

With the B-chamber pressure simplification, the change in pressure within the B-chamber is effectively 0, meaning that the differential equation describing the B-chamber pressure has no effect on the system. This results in the B-chamber pressure state: $\dot{P}_B$ being removed, and all equations that include the B-chamber pressure will have P_B replaced with P_s. The changes are shown in equations (2.56) and (2.57).

$$F_{cyl} = P_A \cdot A_A - P_s \cdot A_B \tag{2.56}$$

$$Q_{leak} = C_{leak} \cdot (P_A - P_s) \tag{2.57}$$

Apart from the changes mentioned in this subsection, the state space system remains the same as in equation (2.51) on page 19. The pressure simplification makes a significant difference, as it decreases the matrix sizes, and thereby the complexity of the state space model. The state space model developed for the case of piston extension is shown in equation (2.58).

$$\begin{aligned}
\begin{bmatrix} \dot{P}_{Af} \\ \dot{\phi}_{pf} \\ \ddot{\phi}_{pf} \end{bmatrix} &= \begin{bmatrix} a_{1,x>0} & a_2 & a_3 \\ 0 & 0 & 1 \\ a_7 & a_9 & a_{10} \end{bmatrix} \begin{bmatrix} P_A \\ \phi_p \\ \dot{\phi}_p \end{bmatrix} + \begin{bmatrix} b_1 \\ 0 \\ 0 \end{bmatrix} x_v \\
y &= C \begin{bmatrix} P_A \\ \phi_p \\ \dot{\phi}_p \end{bmatrix}
\end{aligned} \tag{2.58}$$

3 Linear Model Validation

To validate the linear model, the state space model is run together with the nonlinear system constructed in Simulink. They will be given the same inputs, and will both be running in open loop. Initially, the models will follow a trajectory designed specifically for testing, as this may make it easier spot errors. The first test is a comparison between outputs from the non-linear model and the outputs from the linear model of the case where the hydraulic actuator is retracting the rod. The trajectory used for this case starts at a -5% opening, after which the valve steps an additional -5% in order to determine dynamics when introduced to small changes in valve opening. The linear model is linearized to an operating point based on the non-linear model, running with the same input as the linear model. The operating point is taken when the pressures have reached somewhat steady state, resulting in the velocity state also being somewhat steady, but the position state is not. This operating point is chosen since it is close to steady state for most states, while the system is pitching in the direction which the model is developed for. The trajectory used in the initial test can be seen in figure 3.1.

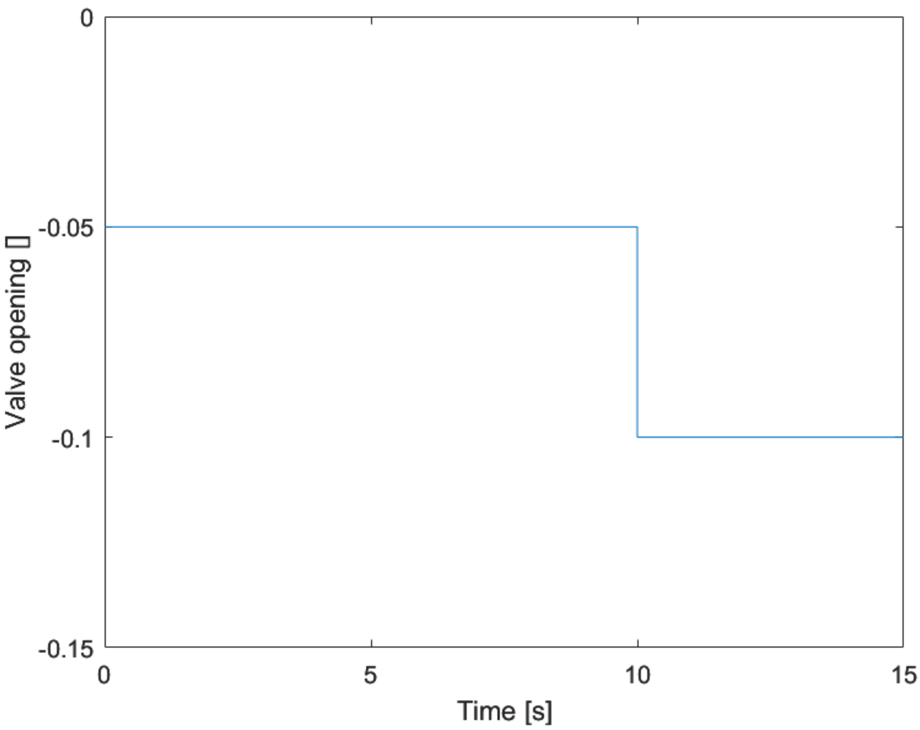

Figure 3.1. *Reference trajectory.*

It can be seen that the valve trajectory runs 10 seconds at its starting configuration, and then 5 seconds after the step. The initial 10 seconds are included to spot potential deviations around the operating point.

The linear model designed with $x_v < 0$ is then compared with the nonlinear model angle output in figure 3.2.

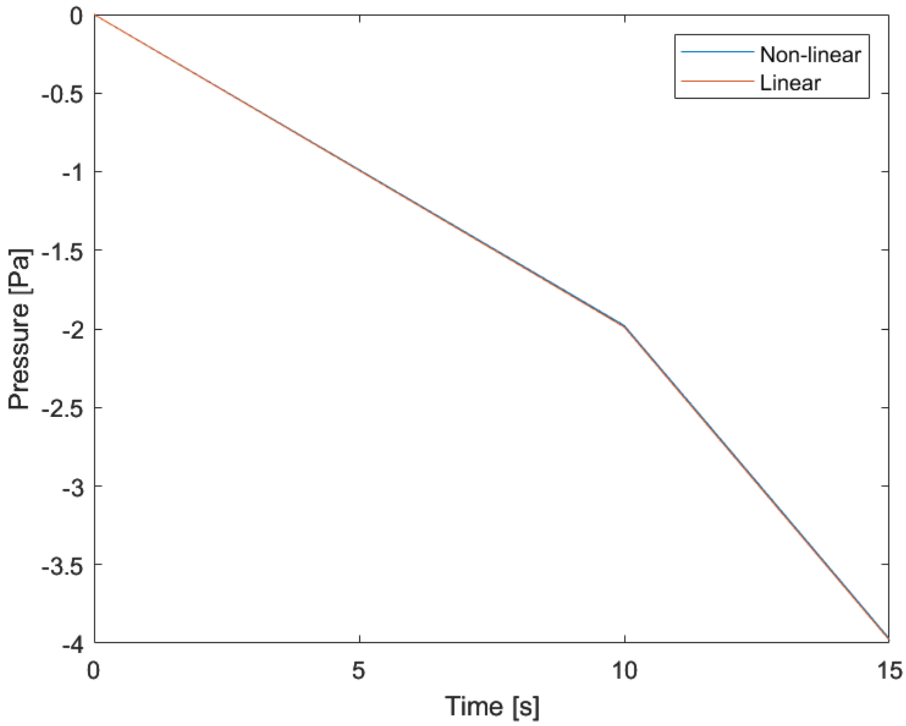

Figure 3.2. *Comparison of model pitch outputs.*

The graph shows that the linear approximation of the pitch, follows the non-linear pitch output very well, with no clearly visible deviations. However, the accuracy of this estimation will decrease the farther from the operating point the system goes. These inaccuracies will not be significant when the linear model is used in the Kalman filter, as the Kalman filter will continuously linearize the model to its current operating point.

Next, the pitch velocities of the two models are compared. The pitch velocity results of the models can be seen in figure 3.3 on the next page.

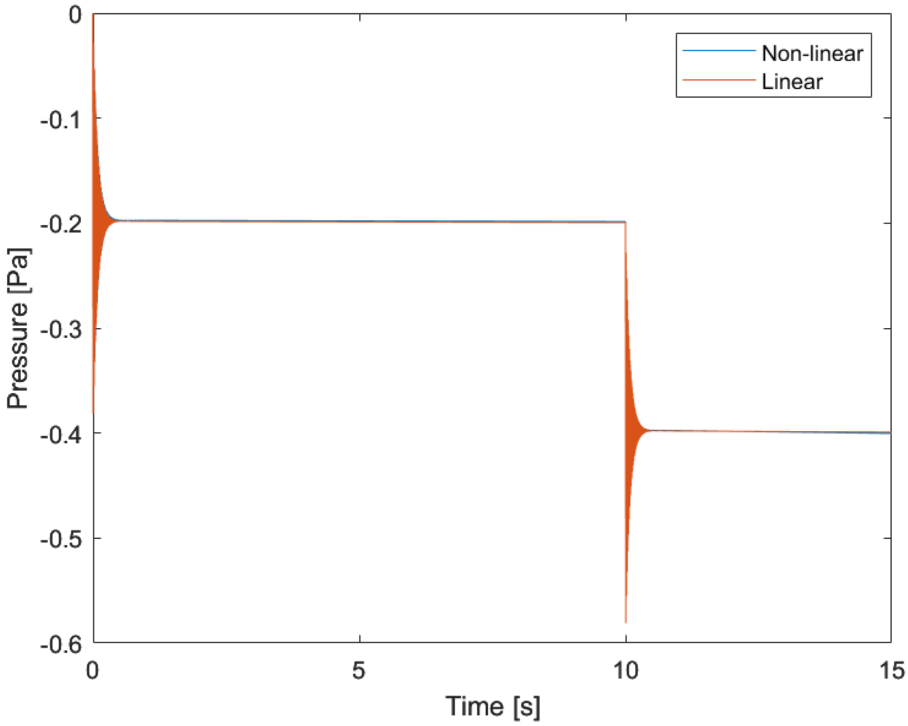

Figure 3.3. *Comparison of model pitch velocity outputs.*

As might be expected from the pitch position results, the pitch velocity results from the two models also follow each other similarly well. The oscillations present at the start and at the step are examined, and it is seen that the models deviate somewhat in their dynamics. However, seeing as the deviations are slight and since the pitch is still well approximated, it is deemed sufficiently accurate.

Next, the two pressures of the chambers will be compared between the two models. Graphs showing the pressure results from both models can be seen in figures 3.4 and 3.5 on the facing page.

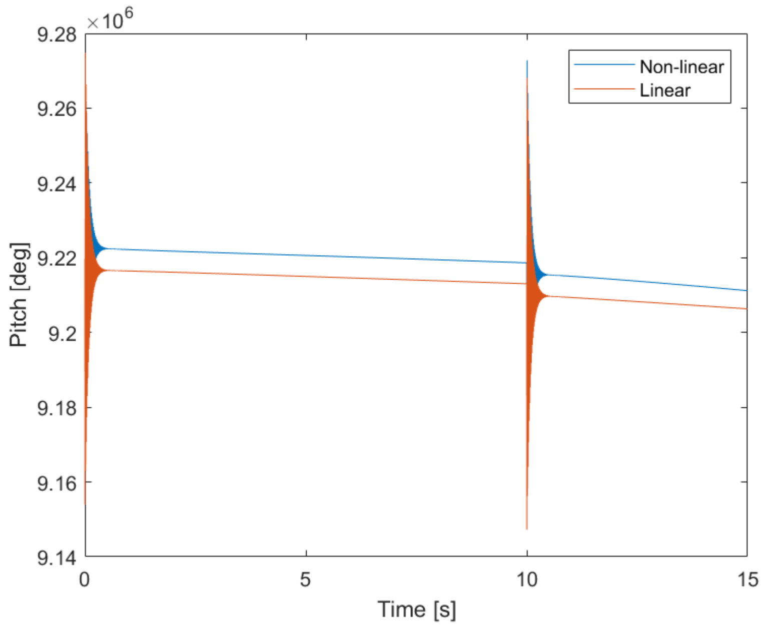

Figure 3.4. *Comparison of model A-chamber pressure outputs.*

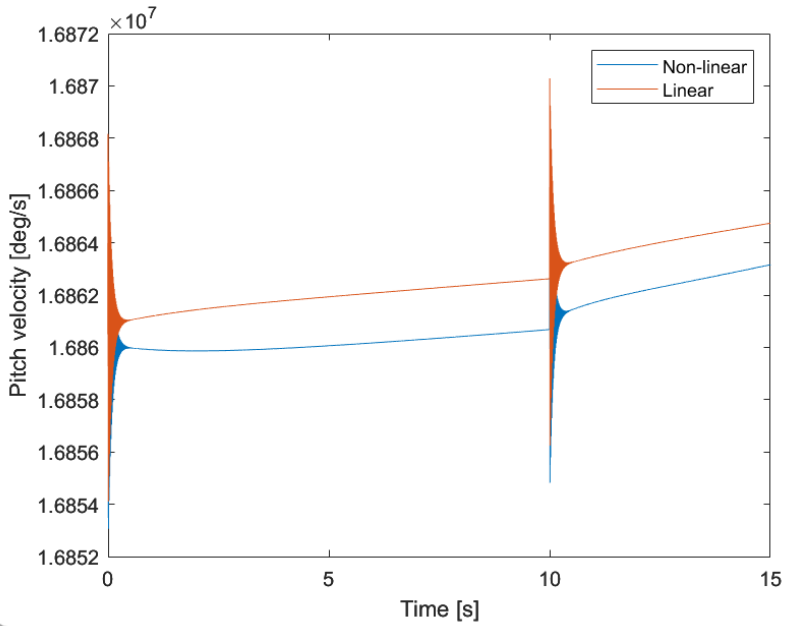

Figure 3.5. *Comparison of model B-chamber pressure outputs.*

The two graphs show that the pressures of the linear model have slightly higher values than the pressures of the non-linear model. This is likely due to some inaccuracies in the initial values of the models as it is seen that the pressures generally follow the same dynamics. It is also seen that the approximated values deviate increasingly as the system moves away from the linearization point. In general the accuracy is deemed sufficient, despite not being completely accurate, as the Kalman filter should be able to correct small discrepancies.

The linear state space model is in general deemed sufficiently validated for use the Kalman filter, and will be included in the Kalman filter tests shown in chapter 4 on page 32.

3.1 State Space Error Investigation

Given that the EKF in section 4.3 on page 37 has diverging covariance matrices, the linear state space model suspected of being inaccurate. This section will cover the considerations, methods and conclusions made to find and fix the underlying problem.

There are different types of errors that could cause a linear model to become inaccurate, and a number of methods in which to investigate and fix the underlying problem. This subsection will list the different methods and considerations that have been used to try and fix the linear model and improve its accuracy so that it may be used in the Kalman filter.

A potential error source could be the parameters used, and the simplifications made prior to linearization. If the parameters used in the non-linear model differ between the two models it would create inaccuracies. However, in most cases, simple discrepancies in parameters would result in increased or decreased dynamics. Because of this, all parameters used in both models are carefully examined, but no parameters were found to differ between the two models. Something else that could have significant effects on the system dynamics, is the simplifications that were introduced for the linearization. In order to test whether these simplifications are causing the errors, the linear model was recreated without said simplifications.

Another potential error source may be the linearization method. The method used in this case is the first order Taylor expansion, which is a method that is often used for linearization, and has proven useful in previous projects. However, there are different ways in which the first order Taylor approximation can be constructed. The way the model is linearized in this case, was using the describing equations of the system and inserting all functions that may be included into the equation itself. This creates three relatively complex equations, that are then used to calculate the partial derivatives used in the state space model. This follows the first order Taylor expansion method, but the complexity of the equations may increase the likelihood of calculation errors potentially introduced by the calculation software. The likelihood of this being the case is unknown, but there are different ways to linearize the model that may avoid this potential issue. One of which is to manually do the calculation, but seeing as this is time consuming and has an increased likelihood of errors, it is not a preferred solution. An alternative would be to linearize the smaller functions included in the main describing equations individually, before inserting them into the main equations. This way, the linearizations can be analyzed for inaccuracies before being inserted into the main equations.

Starting at the A-chamber pressure change, the describing differential equation was shown in equation (2.16) on page 14. This equation is depending on three different states for its calculation as well as the input. The equation contains two variables denoting other equations, the first being the A-chamber flow and the second being the cylinder piston velocity. The A-chamber flow contains the A-chamber pressure and the input, and linearization of this equation is performed as previously mentioned, and shown in equation (3.1) on the facing page.

$$Q_{A,lin} \approx Q_A(P_{A0}, x_{v0}) + \left.\frac{\partial Q_A}{\partial P_A}\right|_{P_{A0},x_{v0}} (P_A - P_{A0}) + \left.\frac{\partial Q_A}{\partial x_v}\right|_{P_{A0},x_{v0}} (x_v - x_{v0}) \tag{3.1}$$

The values for P_A and x_v are supplied directly from the non-linear model. As such, the linear approximation should follow the flow from the non-linear model, as long as the system is operating close to the linearization point, which is the same point as used in the state space model validation. The linear approximation is compared with the non-linear flow in a graph shown in figure 3.6.

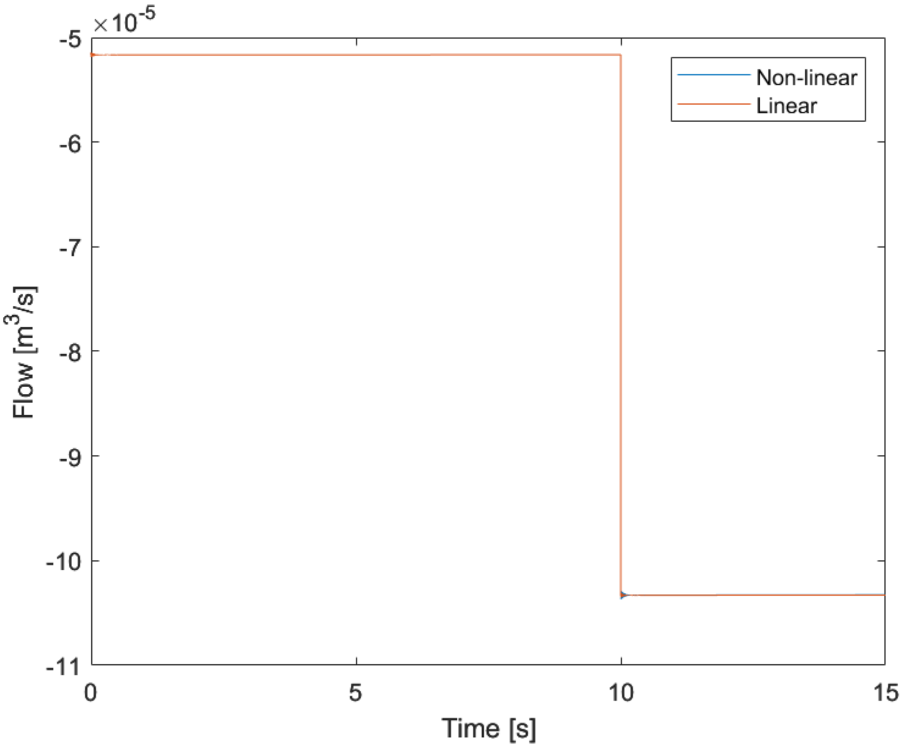

Figure 3.6. *Flow comparison.*

It can be seen from the graph that the approximated flow generally follows the actual flow. Dynamics are present at two points, at the start and at the step. Two additional graphs focused on these points are shown in figures 3.7 and 3.8.

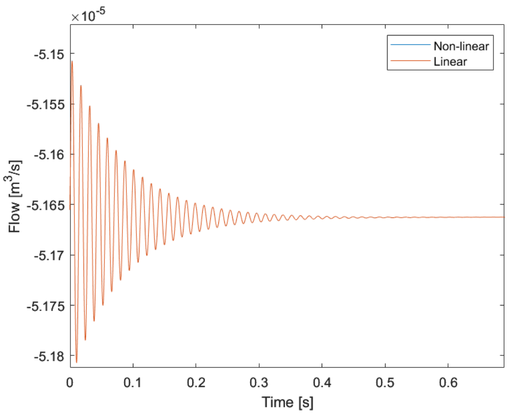

Figure 3.7. *Flow comparison at the start.*

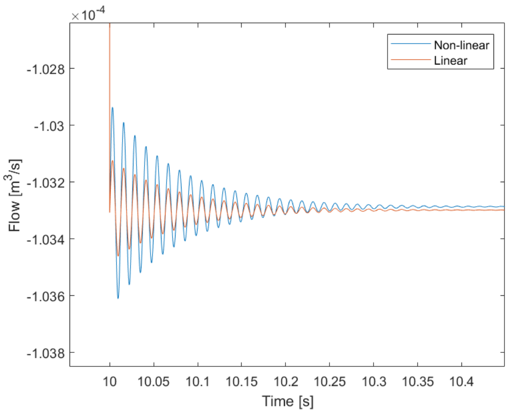

Figure 3.8. *Flow comparison at the step.*

It can be seen that the approximation follows the actual flow exactly at the start, but shows some minor deviations at the step. This is due to the start being closer to the operating point, and the step moving the system away from said point. The difference in dynamics can be explained through differing calculations in the two models. As the system moves the pitch and the piston position in the negative direction, the available volume in the A-chamber will shrink, according the non-linear equation describing the volume. This causes the pressure to increase which consequently causes the flow to increase as well. In the linear equation of volume, the volume change as a factor of cylinder position was removed as a simplification, and replaced with a constant value. The consequence of this, is the difference shown in figure 3.8 on the previous page. As such, the approximation follows the actual flow as expected. The next equation to be linearized is the cylinder piston velocity, which is linearized following the same method as with the flow. The result is compared with the non-linear model, focused at the step as this shows the dynamics, seen in figure 3.9.

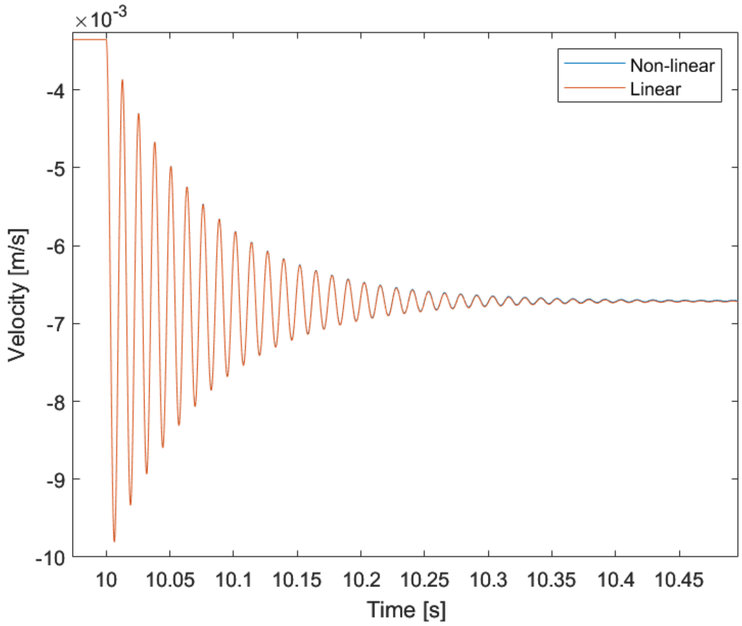

Figure 3.9. *Piston velocity comparison, at the step.*

It can be seen that the approximated velocity follows the dynamics of the non-linear model almost perfectly. This is deemed sufficiently accurate. It is also observed that the approximated velocity drifts in the negative direction after the step. Some additional deviations can be seen in figure 3.10 on the next page. This is caused by the linearization and the deviation will have an effect on the final pressure values.

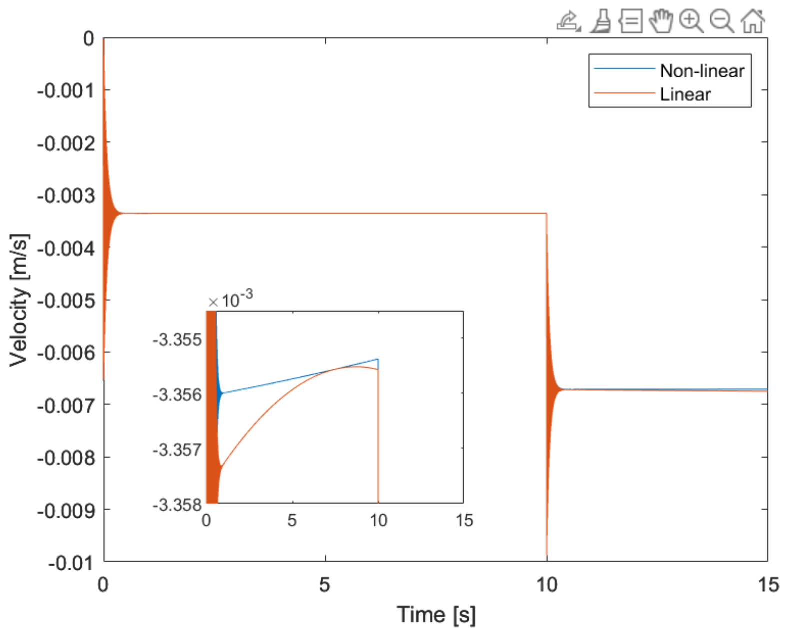

Figure 3.10. *Piston velocity comparison, full view.*

Having linearized the cylinder velocity, it can be used to acquire the linearized cylinder position through integration of the velocity. The position can then be compared to the position measured from the non-linear model, to determine whether the velocity has become inaccurate due to the linearization. The comparison can be seen in figure 3.11.

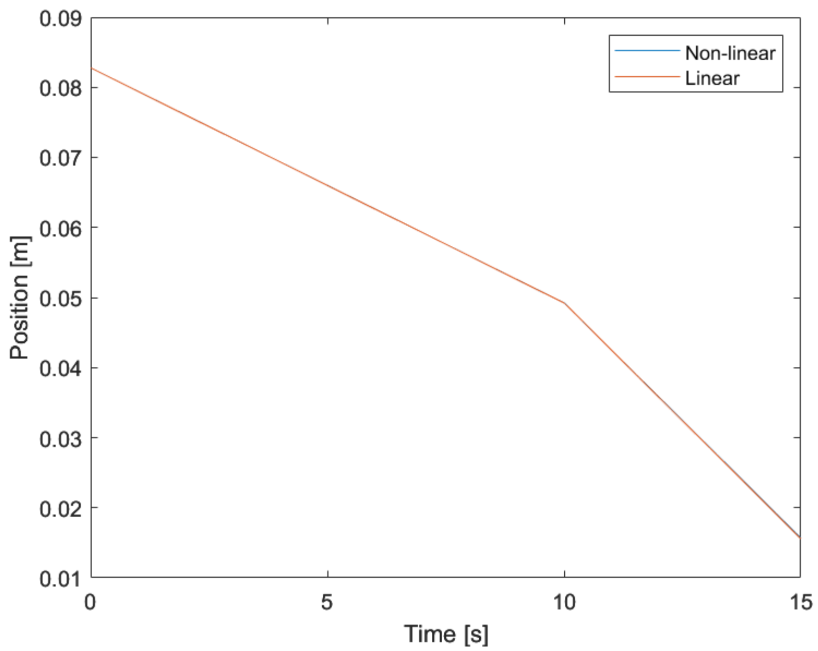

Figure 3.11. *Piston position comparison.*

It is clear that the piston position is approximated well, when operating somewhat close to the operating point.

Having deemed the linearized flow and cylinder velocity generally accurate, the resulting linearized values can be inserted into the pressure change equation, shown in equation (3.2).

$$\dot{P}_{A,lin} = \frac{\beta}{V_{A0} + x_{cyl}A_a}(Q_{A,lin} - A_a\dot{x}_{cyl,lin}) \tag{3.2}$$

Seeing as the equation is now linear, the resulting pressure change will also be linear. The linear pressure change is compared to the non-linear model in figure 3.12. Additionally, integrating the pressure change will output the pressure in the A-chamber. This pressure is also compared between the approximation and the actual pressure values, shown in figure 3.13.

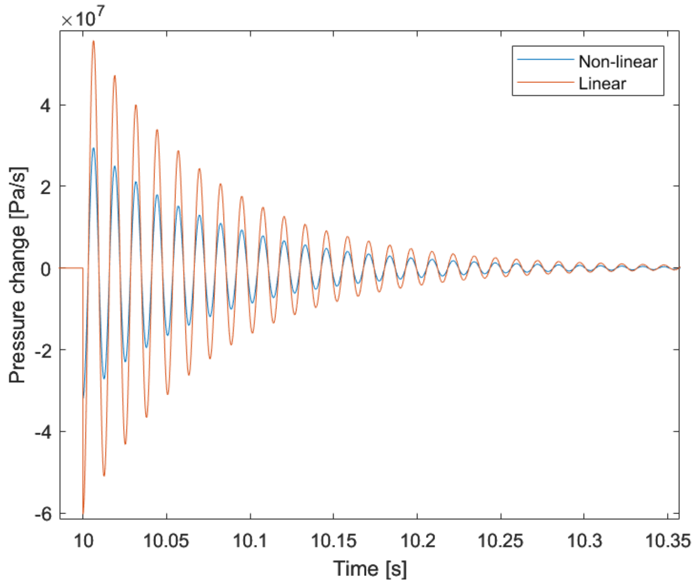

Figure 3.12. *Comparison of A-chamber pressure changes at the step.*

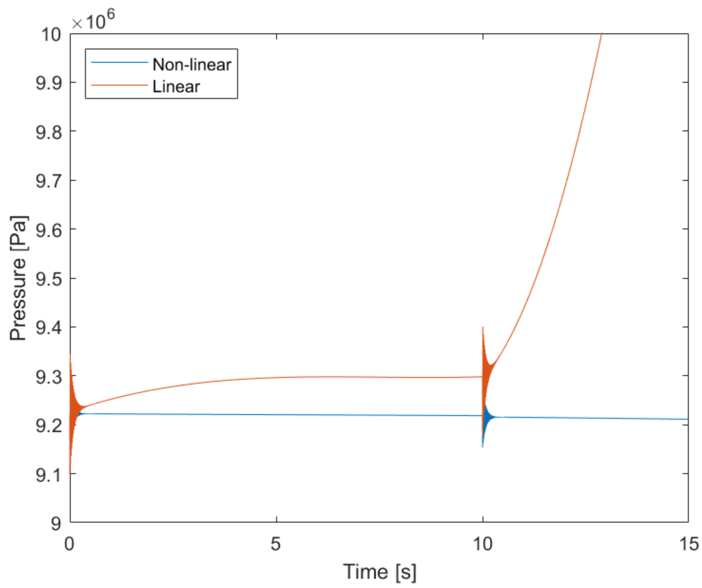

Figure 3.13. *Comparison of A-chamber pressures.*

It is seen that the approximated pressure is larger than the actual pressure, and that it deviates significantly after the step. This is caused by the deviations seen in the piston velocity. A lower piston velocity, results in a larger pressure change. This is also the reason for the deviations in the dynamics of the pressure change shown in figure 3.12 on the facing page. When closely examining the velocity, it is found that the approximated velocity is slightly lower than the actual velocity, differing by around $-0.2 \cdot 10^{-3}$. This slight deviation becomes a large deviation as the flows are multiplied with the bulk modulus, which has a huge value in comparison. The slight deviation of $0.2 \cdot 10^{-3}$ becomes a deviation of $1.96 \cdot 10^{6}$ when run through the linearized pressure change equation. The dynamics of the resulting pressures is also analysed for potential deviations, and the graph comparison used for this purpose is seen in figure 3.14.

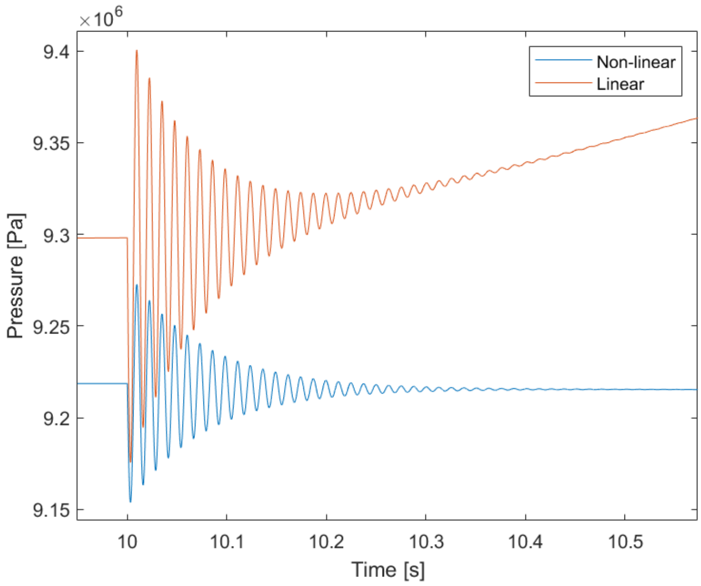

Figure 3.14. *Comparison of A-chamber pressures at the step.*

The approximated pressure is seen to have larger amplitudes than the non-linear pressure, which can be attributed to the velocity as mentioned before, as well as the approximated pressure having a larger value at the step. Apart from this, the frequencies of the pressure oscillations are the same, showing that the dynamics are very similar.

With the A-chamber pressure change equation linearized, and shown to approximate the nonlinear model well, the linear approximation is deemed sufficiently accurate. Even though the approximations are deemed accurate, deviations were observed and largely attributed to the simplifications introduced for the purpose of linearization. The simplifications include the constant bulk modulus and the constant volume of the chamber. Since these simplifications appear to have a somewhat significant influence on the system, including these in the non-linear equations used for the Kalman filter predictions will likely help eliminate the divergence of the covariance matrices. Inclusion of the simplifications is performed in section 4.4 on page 38 before further error investigation is performed.

Extended Kalman Filter Condition Monitoring 4

An extended Kalman filter is a nonlinear version of the usual Kalman filter. Using a model of the nonlinear system, an input of values from the nonlinear model, and estimates of the covariance, the EKF will be able to make estimates of the system states. The EKF linearizes the nonlinear system to currently measured values at every time step, updating estimates as i runs, and uses the previous estimates in the nest estimations.

4.1 Extended Kalman Filter Formulation

The EKF is divided into two steps, with the first being the prediction step and the second being the correction step. The prediction step uses the nonlinear model and the previous corrected estimate to make a new estimate for the next time step. The prediction also estimates the associated covariance matrix. With the predictions made, the EKF begins the correction step, which uses the predicted states and covariance matrix together with the actual measurements, to update the estimates. The updated estimates are, as such, "corrected", and are then used in the prediction step of the next time step. The corrected states are also the outputs of the EKF, and can then be used to compute residuals for condition monitoring. [7]

The prediction step uses two equations. The first equation is used to predict the next state estimate $\hat{x}^-$, and is shown in equation (4.1). The second equation is used to predict the state error covariance P^-, and is shown in equation (4.2). [7]

$$\hat{x}^- = F_{nonL} \tag{4.1}$$

$$P^- = AP^+A^T + Q \tag{4.2}$$

Where P^+ is the state estimate error covariance acquired from the previous correction step, Q is the process noise covariance and A is the system matrix developed for the system.

P^- is a prediction of the state error covariance. It is calculated based on the state error covariance acquired in the last step, which is run through the system matrix and summed with the process noise covariance. The process noise covariance denotes the noise disturbance that would be applied throughout the process of the real system, and it is assumed to be Gaussian with a mean at zero. This covariance can be difficult to obtain, and since this case does not have an experimental setup, the covariance can be freely defined within reason.

The correction step uses three different equations, where the first is used to calculate the Kalman gain K, and is shown in equation (4.3). The second equation calculates the corrected/updated state estimate $\hat{x}^+$, and is shown in equation (4.4). The third and last equation calculates the corrected/updated estimate of the state error covariance P^+, shown in equation (4.5). [7]

$$K = P^- C^T [C P^- C^T + N]^{-1} \tag{4.3}$$

$$\hat{x}^+ = \hat{x}^- + K[y - C\hat{x}^-] \tag{4.4}$$

$$P^+ = [I - KC]P^- \tag{4.5}$$

Where C is the output matrix of the system and , N is the measurement noise covariance, y is a measurement of value(s) from the nonlinear system, and I is an identity matrix.

The Kalman gain essentially determines how much the state estimate relies on either the model or the measurements. If the Kalman gain is low, the estimate will rely mostly on the model estimates, whereas if the gain is high, the estimate will rely mostly on the measurements. The Kalman gain is based on the estimated state error covariance and the measurement noise covariance, which means that a high estimation of state error covariance will likely result in a higher Kalman gain. The measurement noise covariance is similar to the process noise covariance, with the former being based on the measurement noise instead. This covariance can also be difficult to obtain, and will be freely defined, like the process noise covariance was

When the state error covariance is corrected, it is based on the estimated state error covariance and the Kalman gain. This creates a loop in which the state covariance error is propagated, which optimally will converge over time.

All the filter equations are run in a loop, separated into the aforementioned steps. A visual representation of the extended Kalman filter is seen in figure 4.1.

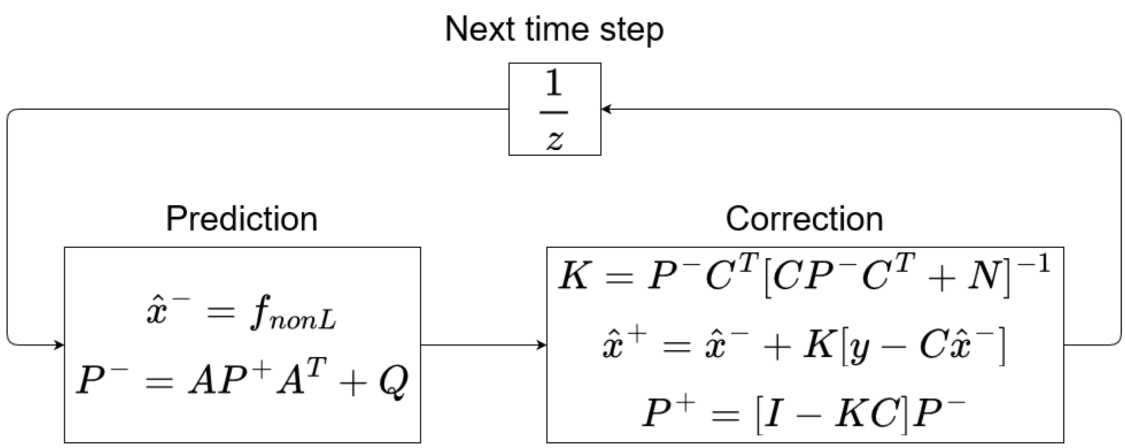

Figure 4.1. *EKF algorithm block diagram.*

With the EKF being based on steps and placed in a loop, it will have to run in a discrete manner, meaning that any equations included from system models will need to be discretized as well. This will include the system differential equations F_{nonL}, as well as the system matrix: A. Discretizing the system differential equations can be done as shown in equation (4.6).

$$F_{discr} = F_{nonL} \cdot T_s + x \tag{4.6}$$

Where T_s is the step size used by the Kalman filter. Having discretized the system differential equations, the system matrix will also need to be discretized. One way to do so, is to apply an exponential function to the continuous system matrix multiplied with the step size

$$A_{discr} = \left.\frac{\partial F_{discr}(X)}{\partial X}\right|_{\hat{x}^+} \tag{4.7}$$

4.2 Leakage Model

The main purpose of the EKF in this case, is to estimate the leakage occurring in the hydraulic cylinder. This can include internal leakage between the two chambers and external leakage due to wear or production errors. However, for the EKF to be able to so, the model used by the EKF will need to have the leakage included in the model. One way to model the internal leakage of a hydraulic cylinder is shown in equation (4.8) [4].

$$Q_{leak} = K_{leak} \cdot (P_A - P_B) \tag{4.8}$$

Where K_{leak} is the leakage coefficient. As such, the leakage flow will depend on the pressure difference between the two chambers and the leakage coefficient, which acts as an expression of the failures in the seal. This leakage flow will be included in the continuity equations as shown in equations (4.9) and (4.10).

$$\dot{P}_{Af} = \frac{\beta}{V_{A0} + x_{cyl} A_a}(Q_A - A_a \dot{x}_{cyl} - Q_{leak}) \tag{4.9}$$

$$\dot{P}_{Bf} = \frac{\beta}{V_{B0} + x_{cyl} A_b}(A_b \dot{x}_{cyl} - Q_B + Q_{leak}) \tag{4.10}$$

This shows that positive leakage flow represents flow from the A-chamber to the B-chamber, as determined by the pressure difference. This leakage will also have to be included in the linear model. The introduction of leakage flow will significantly change the dynamics of the system, since the two pressures will now have direct influences on each other, instead of just an indirect influence. Apart from this, the leakage coefficient will be added to the state vector as a new state, as this will allow the EKF to output an estimation of the internal leakage state. Because of this, the state vector will be changed as seen in equation (4.11).

$$X = \begin{bmatrix} P_A \\ P_B \\ \phi_p \\ \dot{\phi}_p \\ K_{leak} \end{bmatrix} \tag{4.11}$$

The changes introduced by the addition of internal leakage, only has a direct influence on the continuity equations. This also affects the linear model, resulting in new partial derivatives, which are shown in equations (4.12) to (4.15) on the next page.

$$\frac{\partial \dot{P}_A}{\partial P_A} = -\frac{\beta \cdot (K_{leak} - \frac{\partial Q_A}{\partial P_A})}{V_{A0}} \quad (4.12) \qquad \frac{\partial \dot{P}_B}{\partial P_B} = -\frac{\beta \cdot (K_{leak} + \frac{\partial Q_B}{\partial P_B})}{V_{B0}} \quad (4.13)$$

$$\frac{\partial \dot{P}_A}{\partial K_{leak}} = -\frac{\beta \cdot (P_A - P_B)}{V_{A0}} \quad (4.14) \qquad \frac{\partial \dot{P}_B}{\partial K_{leak}} = \frac{\beta \cdot (P_A - P_B)}{V_{B0}} \quad (4.15)$$

These partial derivatives are then used together with the rest of the previously calculated partial derivatives to create a new state space model, using the same method as in section 2.4.3 on page 19. This results in the state space matrices shown in equation (4.16).

$$\begin{aligned}
\begin{bmatrix} \dot{P}_{Af} \\ \dot{P}_{Bf} \\ \dot{\phi}_{pf} \\ \ddot{\phi}_{pf} \\ \dot{K}_{leak} \end{bmatrix} &= \begin{bmatrix} a_1 & a_2 & a_3 & a_4 & a_5 \\ a_6 & a_7 & a_8 & a_9 & a_{10} \\ 0 & 0 & 0 & 1 & 0 \\ a_{11} & a_{12} & a_{13} & a_{14} & 0 \\ 0 & 0 & 0 & 0 & 0 \end{bmatrix} \begin{bmatrix} P_A \\ P_B \\ \phi_p \\ \dot{\phi}_p \\ K_{leak} \end{bmatrix} + \begin{bmatrix} b_1 \\ b_2 \\ 0 \\ 0 \\ 0 \end{bmatrix} x_v \\
y &= \begin{bmatrix} 1 & 0 & 0 & 0 & 0 \\ 0 & 1 & 0 & 0 & 0 \\ 0 & 0 & 1 & 0 & 0 \\ 0 & 0 & 0 & 1 & 0 \end{bmatrix} \begin{bmatrix} P_A \\ P_B \\ \phi_p \\ \dot{\phi}_p \\ K_{leak} \end{bmatrix}
\end{aligned} \quad (4.16)$$

Similar calculations are performed for the case where the proportional valve is in a positive position. From equation (4.16) it can be seen that the output matrix does not output the leakage estimation. This is due to the fact that the leakage does not have any describing equation, and since it is never directly calculated or measured during operation. The leakage is however estimated in the Kalman filter through the use of measured and estimated values of the other states. If the measured states are changing throughout operation in a way that indicate leakage in the cylinder, the Kalman filter will use this to estimate the leakage currently present, but with an accuracy that is dependant on the accuracy of the linear model, and the tuning and precision of the Kalman filter covariance matrices.

With a model of internal leakage developed for estimation, an additional model for estimation of external leakage may also be advantageous, allowing for additional fault detection. A rough estimation of external leakage would be to use an equation similar to equation (4.8) on the previous page. Using the same approach, it is possible to obtain an estimation of external leakage by using the chamber pressure in the cylinder, and the outside pressure, which in most cases can be assumed to be atmospheric pressure. Using these pressures in equation (4.8) on the preceding page will result in an estimation of the external leakage, as seen in equations (4.17) and (4.18) on the next page.

$$Q_{AL,ext} = K_{AL,ext} \cdot (P_A - P_{atm}) \quad (4.17) \qquad Q_{BL,ext} = K_{BL,ext} \cdot (P_B - P_{atm}) \quad (4.18)$$

The implementation of the external leakage in the model, is similar to the implementation of the internal leakage. The leakage flow is included in the continuity equations in the same way as the internal leakage, but with external leakage being a negative flow in each chamber.

4.3 Initial EKF Test

Having developed a model including the internal leakage, it can be used in the extended Kalman filter for internal leakage estimation. The resulting EKF made for this estimation is initially tested on the non-linear model, running with a constant load and a controller. The EKF is supplied with the proportional valve position and measurements of all states, except K_{leak}. However, these inputs and measurements will have noise applied to them to simulate measurement noise. This noise, as well as the covariance matrices will have the same noise variance, where the covariance matrices will be diagonal matrices, that can be tuned if necessary.

The initial test starts out with the system staying still at initial position, before introducing an amount of leakage by controlling the K_{leak} of the non-linear model. This leakage appears suddenly with a step, simulating sudden seal failure and applying a large amount of leakage, with K_{leak} being set to 10^{-10}. After 20 seconds, the pitch reference is changed to -1 degrees, setting the system in motion. The EKF should ideally be able to estimate the internal leakage throughout the simulation. Estimation of the other states should preferably also be accurate, as the leakage depends on them, but the leakage is the main focus.

The test resulted in failure, as the Kalman filter stopped outputting values shortly after starting. Some of the results from the test can be seen in figure 4.2.

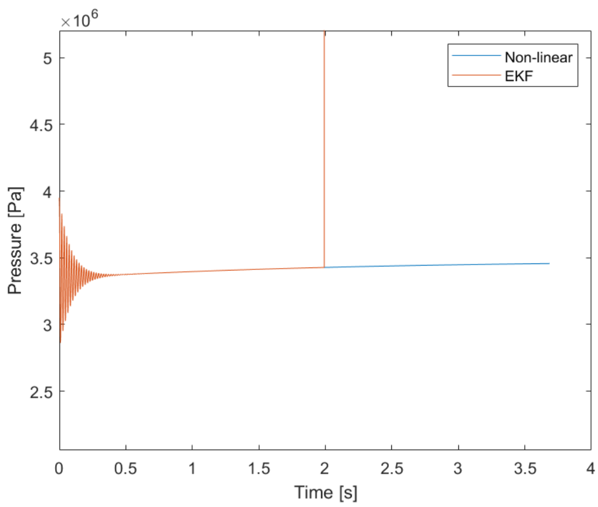

Figure 4.2. *A-chamber pressure results from the model and EKF.*

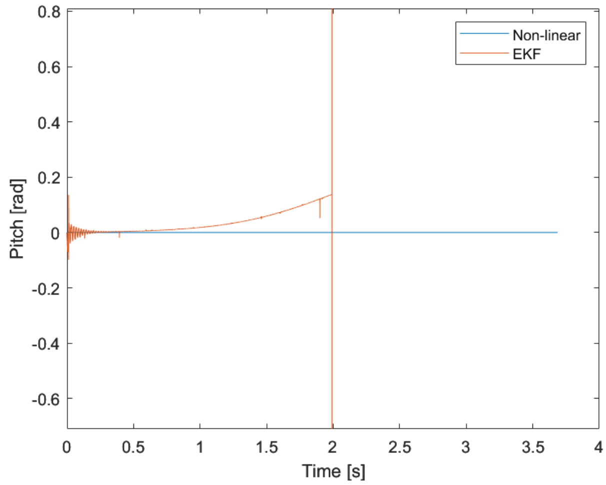

Figure 4.3. *Pitch results from the model and EKF.*

The graphs show that the EKF stops after around 2 seconds. Examination of the EKF when approaching this point shows that the values of the covariance matrices increase significantly over a short amount of time. This divergence results in the values of the covariance matrices increasing beyond the bounds of a double variable, resulting in values that first become infinite, and then they are replaced with NaN (not-a-number), stopping the EKF.

The diverging covariance matrices renders the EKF unusable. Divergence in the EKF can point towards the EKF being poorly configured, or the modelling being poor. As such, the linear model is investigated for errors in section 3.1 on page 26.

4.4 Second EKF Test

In section 3.1 on page 26 it was found that the simplifications made for linearization were significant for the system. Including the simplifications in the non-linear equations that the EKF uses to predict the state estimate, will reduce the differences between the linear and non-linear models, thereby reducing the covariance changes.

The simplifications are included into the estimated state space prediction, and the test is run again, in the same way as in section 4.3. This test performed significantly better, having the EKF run throughout the whole test. The EKF state estimates are compared with the actual states, which can be seen in figures 4.4 to 4.8 on pages 39–41.

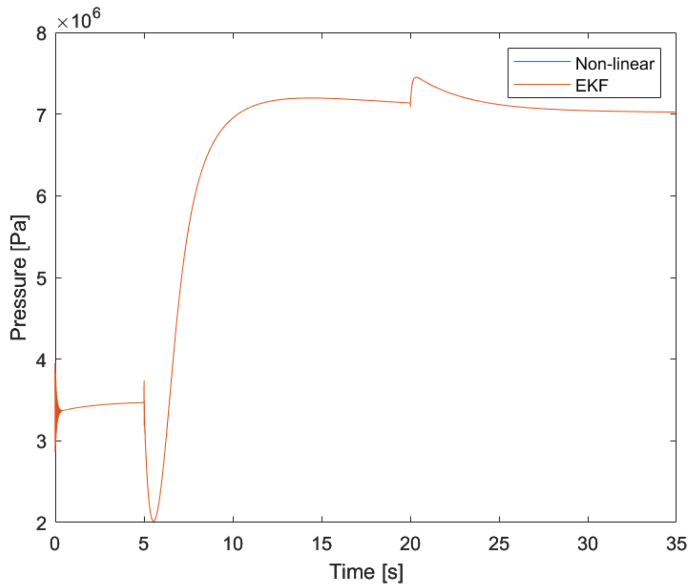

Figure 4.4. *A-chamber pressure comparison from the second test.*

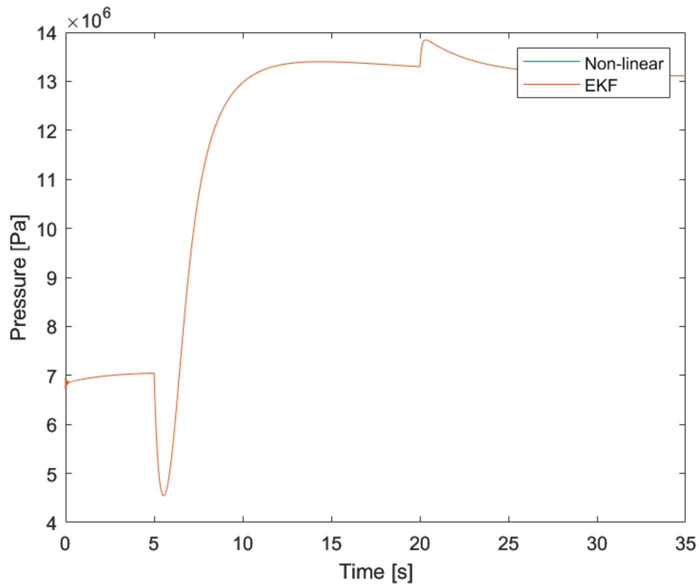

Figure 4.5. *B-chamber pressure comparison from the second test.*

The pressure graphs show that the pressures are very well estimated, following the actual pressures without any significant deviation.

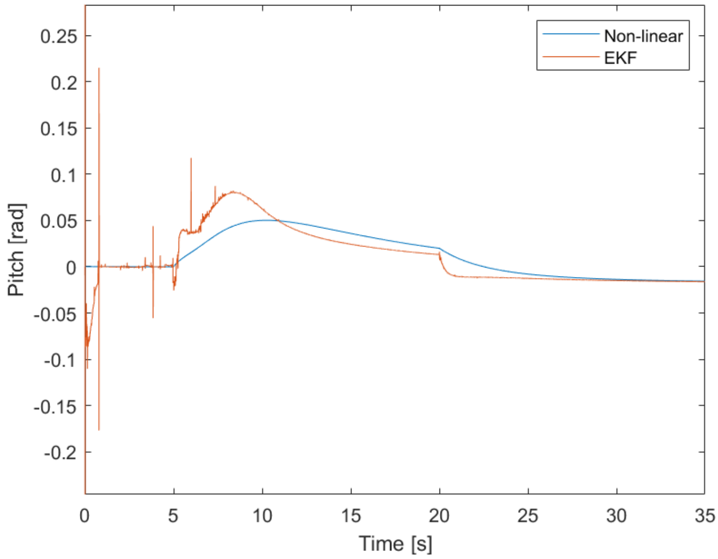

Figure 4.6. *Pitch comparison from the second test.*

The estimated pitch is shown to be inaccurate. Noise is present which result in somewhat large sudden deviations, and the estimated pitch shows different dynamics. The pitch is largely estimated based on its previously estimated position and the pitch velocity. As such, the pitch velocity estimation may be the cause to some of these deviations.

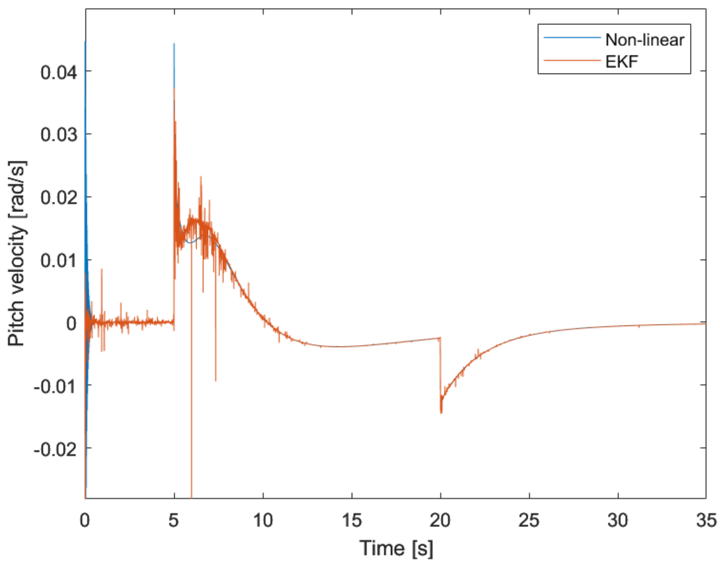

Figure 4.7. *Pitch velocity comparison from the second test.*

The pitch velocity deviation is seen to generally follow the actual velocity, with some deviation when the leak is introduced, and with noise present throughout most of the test. The deviations appear when the leakage is introduced, but disappear over time. These deviations will influence the estimated pitch, producing deviations in that estimate as well.

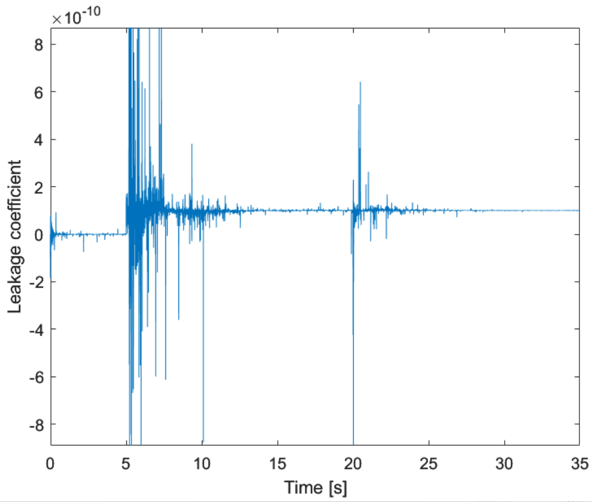

Figure 4.8. *Estimation of leakage coefficient.*

The estimated leakage coefficient is seen to estimate the leakage introduced on the non-linear model with decent accuracy, but with a large amount of noise present. The general estimation of the leakage is seen to change at the 5 second mark, at which the leakage was introduced. The estimation settles around a leakage coefficient value of around 10^{-10} which is the exact value at which the leakage coefficient is set to in the non-linear model. As such, the EKF is able to estimate the leakage present in the system, however with noise obscuring the general estimation. The quality and usefulness of this is discussed in

5 Discussion

Seeing as there has been an amount of problems during model development and Kalman filter performance, there is a number of observations, choices and assumptions that should be accounted for and discussed.

The model was validated against the pitch position, proportional valve input and load torque based on load pressures supplied by a piston that is only part of the experimental setup. With these parameters validated sufficiently, the pitch position calculated by the model could be deemed realistic, but the pressures making up a large part of the dynamics of the system did not have data to validate against. As such, the pressure dynamics may not be completely trustworthy, as there was no data to compare it with. It can be argued that the model is sufficiently accurate if it follows the general behaviour of the limited data set.

The state space model was constructed from the non-linear model, with the same parameters and their corresponding units. This means that pressures are expressed in pascal and that the pressures have very large values compared to the rest of the unit values present in the model. This consequently means that a small input introduced by the control valve, will result in comparatively large changes in the system matrix. This may result in the system matrix becoming ill-conditioned, which can have adverse effects on the model, if any error is present.

The results acquired from the second EKF test, showed that the EKF is able to estimate the internal leakage. However some of the results, including the estimated leakage, included an amount of noise. This noise can be removed in a few ways. One way would be to filter the estimated values to remove outliers and some amount of noise. Alternatively, the EKF can be tuned to improve estimations, by tuning the variances used in the covariance matrices of the EKF. This is a preferable solution as it increases the accuracy of EKF estimations.

The usefulness of the current EKF results can be discussed. If the estimated leakage coefficient is filtered effectively, the estimation becomes relatively trustworthy, according to the tests performed. Analysing the leakage coefficient and how it changes can then be useful for determining when the leakage will reach a critical level. Implementing an algorithm to do this will make it possible to automate the condition monitoring, by using the algorithm to signal that the leakage will reach a custom set limit within a certain time. As such, the EKF can be useful for automatic condition monitoring, but will need refinement and additional algorithms for optimal monitoring. This is not included due to time constraints

6 Conclusion

With the goal of investigating CM methods for the hydraulic actuator of a wind turbine pitch system, the state of the art was investigated. The state of the art highlighted some CM methods that could be used for this goal, and showed both positives and negatives of each method, before choosing to investigate the use of EKF state estimation for CM purposes. The investigation was conducted theoretically and did not involve testing on an actual system.

A non-linear model was developed for the purpose of representing an actual wind turbine system. The model was refined to fit the dynamics of an experimental data set, and succeeded in capturing the general behaviour of a wind turbine pitch system according to the provided data. The data was limited in scope and parameters, meaning the validated model is not confirmed to accurately resemble a wind turbine pitch system in the aspects not included in the data. This makes the model accurate enough for testing, but will need further validation to fit a real system. Since the model functions as the basis system for comparison, the linear model and EKF are also affected by this.

A linear state space model was developed for use in the EKF, and was therefore validated to approximate all states accurately for this purpose. The validation showed adequate accuracy in the approximations, with small deviations that were deemed insignificant for use in the EKF. An analysis of the linearized model was later performed for EKF error investigation, which highlighted a significance in the simplifications introduced during linearization. These simplifications were shown to have a significant influence, and were subsequently inserted into the non-linear state prediction of the EKF, resulting in significant improvements.

An Extended Kalman filter was developed and tested with the non-linear model with the purpose of estimating internal leakage. The initial test ended in failure, as the EKF covariance matrices diverged, resulting in the EKF effectively stopping. Following the analysis of the linear model, and including the simplifications in the non-linear state prediction, the EKF performance was significantly improved. The EKF accurately estimated pressure values, but showed some deviation and noise in estimating the pitch and pitch velocity. The internal leakage estimation was deemed successful, however with significant noise present. It is proposed that the estimation is either filtered additionally, or that the EKF is further tuned to allow for better estimations.

In conclusion, the EKF method is theoretically investigated and shown to be successful in estimating internal leakage, making EKF a valid method for CM of the hydraulic actuator of wind turbine pitch systems. It will need additional algorithms for actual CM and could benefit from additional refinement, tuning and additional testing to ensure that the EKF

CM method is valid for a broad range of cases.

Bibliography

[1] Pierre Tchakoua, René Wamkeue, Mohand Ouhrouche, Fouad Slaoui-Hasnaoui, Tommy Andy Tameghe, and Gabriel Ekemb. Wind turbine condition monitoring: State-of-the-art review, new trends, and future challenges. *Energies*, 7:2595–2630, 2014. doi: https://doi.org/10.3390/en7042595. URL https://www.mdpi.com/1996-1073/7/4/2595.

[2] Jesper Liniger. Design of reliable fluid power pitch systems for wind turbines, 2018.

[3] Leo W. Caspers Vignesh V. Shanbhag, Thomas J. J. Meyer and Rune Schlanbusch. Failure monitoring and predictive maintenance of hydraulic cylinder—state-of-the-art review. *IEEE/ASME TRANSACTIONS ON MECHATRONICS*, 26:3087–3103, 2021. doi: 10.1109/TMECH.2021.3053173. URL https://ieeexplore.ieee.org/document/9329070.

[4] Liang An and Nariman Sepehri. Hydraulic actuator leakage fault detectionusing extended kalman filter. *International Journal of Fluid Power*, 6:41–51, 2005. doi: https://doi.org/10.1080/14399776.2005.10781210. URL https://www.tandfonline.com/doi/abs/10.1080/14399776.2005.10781210.

[5] Anders Hedegaard Hansen. Fluid power systems, 2021.

[6] Torben O. Andersen Henrik C. Pedersen and Jesper Liniger. Investigation of load reduction possibilities in wind turbines using a fluid power pitch system. 2015. doi: http://dx.doi.org/10.1115/FPMC2015-9598. URL https://www.researchgate.net/publication/314596436_Investigation_of_Load_Reduction_Possibilities_in_Wind_Turbines_Using_a_Fluid_Power_Pitch_System.

[7] Jesper Liniger. System identification & diagnosis, 2022. Course held at AAU on 9th semester of MCE.

Parameters A

α	0.001
n	1.4
$beta_0$	1.6^9
P_t	10^5
P_s	$200 * 10^5$
P_c	0.0
K_{cv}	$1.5 * 10^{-8}$
L_{AE}	1.715
L_{AB0}	1.185
L_{BE}	0.985
F_{stat}	4000
F_{vis}	10000
ϕ_0	0.8203
A_a	0.0154
A_b	0.009
V_{A0}	$3.7 * 10^{-4}$
V_{B0}	$1.5 * 10^{-4}$
Q_{nom}	0.00125
P_{nom}	10^5
T_s	0.00005